Nano-indentation Study of the Surface of Ion-Exchanged Lithium Silicate Glass

Courtney Calahoo,[†] Xiaofang Zhang,[‡] and J. W. Zwanziger[*,†]

[†]*Department of Chemistry, Dalhousie University, Halifax, and* [‡]*Department of Biomedical Engineering, Dalhousie University, Halifax*

E-mail: jzwanzig@dal.ca

Phone: +1 902 494 1960. Fax: +1 902 494 1310

Abstract

Variations in mechanical properties (stiffness and hardness) were measured as a function of case depth in ion-exchange glasses using nano-indentation. A simple silicate composition, $30Li_2O$-$70Si_2O$, was exchanged ($Li^+ \leftrightarrow K^+$) at several different temperatures, below and above the glass transition, to evaluate the effect of exchange temperature on mechanical properties throughout the ion-exchange layer. Significant enhancements in Young's modulus and hardness were found near the edge in ion-exchanged glasses and attributed to compressive stress and the mixed-alkali effect. Indent size effect-like behaviours were observed in the untreated and ion-exchange samples alike near the sample edge; this was explained by surface-condition sensitivity and compressive stress found within this region. The elastic recovery and resistance to plastic deformation were calculated to assess the effect of ion exchange on elastic and plastic mechanical responses. Micro-hardness measurements of the exchanged samples were also made for comparison.

[*]To whom correspondence should be addressed

[†]Dalhousie University, Department of Chemistry

[‡]Dalhousie University, Department of Biomedical Engineering

Introduction

Glass has a high theoretical tensile strength, greater than 10 GPa, yet most commercial glass products fail at stresses between 10–100 MPa.[1,2] The reason for this large discrepancy lies in the material's surface condition. If the specimen is acid-etched or fire-polished, an increase of one or two orders of magnitude in strength can be attained; conversely, a purposely scratched surface can reduce strength by at least an order of magnitude.[1,2] Consequently, understanding and improving the mechanical properties of glass *at the surface* has a disproportionately large impact on the applications in which it is currently used; not only can improvements create opportunities for new applications, it can also reduce the amount of material required for current applications and the resulting environmental footprint.

The first step towards understanding the importance of the surface condition was made by Inglis,[3] who proposed that scratches act as stress concentrators where local stresses exceed the ultimate tensile strength of the material, which leads to crack propagation and fracture. Later Griffith[4] expanded upon this idea and for brittle materials described a critical crack length (a) and tensile strength (σ_f); if the flaw length is equal to or larger than a, the material will fail at σ_f. Interestingly, for glass the relationship between surface flaw length and strength is linearly dependent on the material's Young's modulus (Y) and surface energy density, (γ), $a = 2Y\gamma/\pi\sigma_\mathrm{f}^2$.[4] It follows that there are two major ways to improve the breaking strength of glass; either prevent flaws above the critical limit from occurring, such as by the application of a protective polymer coating, or increase the Young's modulus and surface energy density of the material.

Surface energy quantifies the work needed to break the bonds of a material and create two new surfaces, thus a way to increase surface energy density is to increase the bond strength or number of bonds per unit area. Stiffness can be improved similarly by increasing those parameters, which leads to a large portion of glass research focused on creating new stiffer glass compositions. It is also possible to strengthen glass only at the surface, without needing a new composition, using thermal tempering or ion-exchange (IE). These processes

create compressive stress at the surface, which counteracts the concentrated tensile stress at crack tips responsible for fracture. Both processes improve the mechanical properties, however, IE creates larger stresses over a shallower depth and has the additional qualities that it can be used to strengthen irregularly-shaped or thin (<1 mm) objects.[5] Specifically, IE has been shown to increase the flexural strength of materials damaged by contact loads up to 40 N by 2–4 times[5] and hardness by 8-40%.[6,7] As a result, IE is used heavily in high-stress applications within many fields, such as safety, medical, optics and the electronic industries.[5,8–10]

The IE procedure requires immersing the sample in a molten bath of alkali salt and permitting smaller ions within the glass sample to exchange with larger ions in the bath, while remaining below the glass transition temperature, T_g. Typically, Na^+ or Li^+ are exchanged for K^+, creating compression by forcing a larger ion into a "smaller" site while preventing structural relaxation from occurring. There have been experimental[9,11] and computational[12,13] investigations of the structure of the glass after the IE process. Additionally, studies have measured the compression at the surface; depending on the length and temperature of the treatment stresses between 100–1000 MPa can be found for case depths between 20–1000 μm (case depth is originally a metallurgical term describing the hardened protective layer which encases the material after IE).[5,7,14–16] Although the mechanical advantages of the IE process are well-exploited, the elastic properties *at the surface* are not well-characterized. The goal of this paper is to establish the effect of compressive stress and compositional variation on the mechanical properties stiffness and hardness *within the IE layer*. Given the significance of the surface condition with respect to breaking strength, it is important to understand how the IE process and resulting compression change both the elastic and plastic response of the material at the surface.

Mechanical properties, namely stiffness and hardness, are easily defined for bulk isotropic materials such as glass. In a nano-indentation experiment, stiffness is quantified using Young's modulus, Y, which relates uniaxial stress, σ, to uniaxial strain, ϵ, ($\sigma = Y\epsilon$).[17]

Hardness (H) is a material's resistance to permanent deformation following indentation, formulated as force (F) divided by the *projected* area of the indent (A), $H = F/A$.[17] However, the shape of indenter tip and load of indenter play a large role in the hardness values obtained, which makes it difficult to compare across hardness values. As a result, reported hardness values typically include the type of tip and load in kilogram-force (kgf), simply the weight of the load, however, kgf can be converted to Newtons using the force of gravity, thereby, hardness can be reported in GPa. The Young's moduli and hardnesses of oxide glasses are typically found in the range of 40–100 and 4–10 GPa, respectively.

Although it is expected that IE will improve the stiffness and hardness, it is difficult to know by how much and the reason for this improvement. The treatment has been known to enhance strength,[5] however, as discussed earlier, this property is dependent on several factors, stiffness being only one. On the other hand, hardness of IE glasses has been well-studied and a 8–20% increase is expected.[6] Although both stiffness and hardness pertain to a material's ability to resist deformation, the main difference is that the former is entirely elastic, while the latter contains both elastic and plastic deformation components.[18,19] Nonetheless, because glass is a brittle material indentation mostly probes the elastic response; in fact, Oyen[19] determined from nano-indentation data that the deformation resistance was 84% elastic and 14% plastic for fused silica.

In glasses containing more than one type of alkali, a concurrent reduction in ion mobility[20] and increase in hardness[21] known as the mixed-alkali effect (MAE) is known to occur. We expect that IE produces similar structural changes whereby ion movement is hindered leading to a decrease in plasticity and increase in hardness. Additionally, the compressive stress is likely to limit the mobility of the glass network and ions further, increasing hardness again. In general, the stiffness of a material increases upon compression.[22,23] Additionally, compression increases the effective tensile strength of a material as external tensile forces must perform work against the compression in order to return the material to an unstressed state. Densification of the glass network is expected from IE, likely leading to higher bond

density as well.

As the name implies, nano-indentation can use much smaller loads and produces smaller indents than typical hardness measurements, on the order of 10–100 mN and 10–1000 nm, respectively.[24] In fact, loads of only a nanonewton and displacements of 0.1 nm have been measured accurately.[24,25] These attributes make nano-indentation the clear choice for characterizing the mechanical properties of thin films and surfaces, such as the IE case depth. Unlike traditional hardness testing, which involves indentation and imaging of the indent at a later time, nano- or ultra-low load indentation is able to measure Y and H continuously. It measures the load (P) and displacement into the surface (h) during one complete cycle of loading and unloading, allowing real-time determination of F and A. A small harmonic vibration of the tip is also added to measure the contact stiffness at any point during the indentation. The underlying equations that allow the determination of stiffness and hardness from nano-indentation assume a mostly elastic contact between the indenter tip and sample, resulting in sink-in only (where the material around the indenter deforms below the original surface plane) rather than pile-up of the material around the indent.[25] This is generally a valid assumption for the indentation of hard ceramics[24] and/or glasses.

At low indent loads, such as the 0.5 N (0.05 kgf) used here, the indentation size effect (ISE) has been found to affect hardness measurements in glasses. The ISE has been defined as an increase in hardness at decreasing indent penetration depths, typically beginning below one micron.[26] The effect is thought to be caused by dislocation strengthening (necessary to accommodate plastic deformation) and/or friction between the indenter and specimen.[26–28] Although most publications have focused on the ISE in bulk metallic glasses,[28–30] it has been found to exist, albeit with a small magnitude, in silicate glass and fused quartz.[31–34] Plastic deformation in amorphous metals is known to occur through highly localized "shear bands" rather than dislocations.[28]Interestingly, in the case of IE glasses, an ISE was reported in the Young's modulus and hardness for loads less than 10 and 120 mN, respectively, and hardness for penetration depths less than 500 nm.[6] Consequently, we do not expect to see the ISE in

nano-indentation measurements above these loads and penetration depths.

In order to investigate the effect of ion exchange on mechanical properties *near the surface*, simple binary $30Li_2O$-$70SiO_2$ glasses were prepared and ion-exchanged with K^+ and were subsequently polished upon one face to expose the composition profile of the IE layer. Furthermore, to better understand the temperature dependence and thermal relaxation of stress, the IE procedure was performed at several different temperatures, ranging from well below to above the glass transition temperature, T_g, of the starting composition. Nano-indentation was then performed on the IE glasses to obtain the stiffness and hardness as a function of case depth and IE temperature. Additionally, the corresponding bulk as-melted mixed-alkali series (xLi_2O-$(30-x)K_2O$-$70SiO_2$) was synthesized and its mechanical properties were determined.

Experimental

Glass Preparation

The starting composition, $30Li_2O$-$70SiO_2$ was prepared by melting stoichiometric amounts of Li_2CO_3 ($\geq$ 99%, Sigma-Aldrich) and SiO_2 (purum p.a., Sigma-Aldrich) at 1550 °C in a Pt crucible for 1–2 hrs, followed by quenching in air and annealing at 415 °C for 16 hrs. Using a similar procedure, the compositionally-equivalent, bulk as-melted xLi_2O-$(30-x)K_2O$-$70SiO_2$ series was made for comparison, including dried (400 °C, 2 hrs), granular K_2CO_3 ($\geq$ 99%, ACP) as a starting reagent and an annealing temperature between 415–450 °C. Variations in the annealing temperature were required due to the varying composition, with K_2O-rich samples requiring higher annealing temperatures. Small batches (7 g) were used to minimize rapid bubbling from the decomposition of K_2CO_3 at greater than 800 °C. All glasses were inspected optically using crossed polarizers to ensure homogeneity and the absence of residual stress. Finally, the samples were cut and polished using a final diamond grit of 1 μm.

Bulk Properties

The Young's moduli and Poisson's ratios of the bulk mixed-alkali series were measured using the ultrasonic method; a Panametrics NDT transducer was used to measure the longitudinal and transverse wave velocities. Density was determined using the Archimedean method with absolute ethanol and, along with the velocities of sound, was used to calculate the stiffness. Typically, the error of the stiffness measurements for the bulk series was ≤ 1 GPa. Vicker's hardness measurements were made using a Leco V-100A Hardness Tester with a load of 1 kg for 15 seconds followed by immediate optical analysis of the indents. Typically, 6–8 measurements were made per sample and errors of 10 HV/1 (10 Vicker's hardness units at a load of 1 kg) or 0.1 GPa were observed. Two bulk glass compositions, $30Li_2O$-$70SiO_2$ and $20Li_2O$-$10K_2O$-$70SiO_2$, were analyzed using differential scanning calorimetry to obtain T_g values. A Netzsch DSC 404 F1 Pegasus instrument was used with a heating rate of 10 °C/min in Ar gas; the instrument has a precision of ±2 °C.

Ion-Exchange Procedure

The untreated starting composition, $30Li_2O$-$70SiO_2$, was cut into several pieces, approximately $1 \times 1.5 \times 0.5$ cm, each of which were ion-exchanged in a fresh bath of molten KNO_3 ($\geq$ 99%, APS) at a different IE temperature between 390–480 °C for 72 hours in a N_2 atmosphere. The wide IE temperature range was chosen to span T_g, measured to be 459 °C, while 72 hours was known to produce significant differences in ion penetration depth.[5] After exchange, the samples were inspected optically with cross-polarizers for residual stresses in the bulk. The exchange of ions was confirmed by measuring the mass gain. The IE samples were embedded in a epoxy discs and then the top IE layer was removed by polishing with 30 μm grit sandpaper, thereby exposing the IE layer along the sides of the sample. This procedure allows the compositional profile of the case depth to be probed; it is a "side-view" rather than a top-view approach. The samples were then polished to a final grit of 1 μm. Effort (long polishing times and use of low loads) was made to obtain an even epoxy disc as

well as a level transition between the epoxy-glass interface.

Elemental Analysis

The nominal compositions of the bulk $x\mathrm{Li_2O}$-$(30-x)\mathrm{K_2O}$-$70\mathrm{SiO_2}$ series were confirmed using inductively coupled plasma optical emission spectrometry (ICP-OES) with a precision 0.1 mol-%. On the other hand, the untreated, $30\mathrm{Li_2O}$-$70\mathrm{SiO_2}$, and IE compositions were analyzed using scanning-electron microscopy–wave-dispersive spectroscopy (SEM-WDS) with a JEOL-8200 Superprobe. Sanidine was used as the standard to determine accurate mol fractions of K, Si and O. Only small errors were introduced: for elements ≥ 2 mass-%, error is 0.3 mass-%, while elements < 2 mass-% have errors of 0.2 mass-%. Although WDS cannot detect lithium content directly, $\mathrm{Li_2O}$ concentration was estimated from the concentrations of the other elements, assuming charge balance. Point analyses were performed approximately every 10 ± 1 μm within the case depth.

Nano-Indentation

Nano-indentation was performed at room temperature using an Agilent G200 Nano-indenter using the Agilent Nanosuite G-series, "Continuous stiffness measurement (CSM), standard hardness, modulus and tip cal" module. A calibrated and certified diamond tip Berkovich indenter with a tip radius ≤ 20 nm was used. The surface approach velocity for each indent was 10 $\mathrm{nm{\cdot}sec^{-1}}$, while the allowable drift rate and surface detection (stiffness criteria) were preset to 0.05 $\mathrm{nm{\cdot}sec^{-1}}$ and 200 $\mathrm{N{\cdot}m^{-1}}$, respectively. Y and H were calculated by the software using equations from Oliver and Pharr's seminal paper;[32] when determining Y, a typical Poisson's ratio for glass, 0.3, was assumed for all samples.[35] Although the Poisson's ratio (ν) is likely to be affected by changes in composition and perhaps stress, a significant decrease in ν from 0.3 to 0.25 results in an decrease in Y of only 2.3%, thus, a constant ν is considered to be reasonable.

Indents were made in two configurations: "face-on", perpendicular to the case depth and

"side-view", a cross-section of the case depth. For the cross-section, an angled procedure was used (as shown in Fig. 1) where an angle of 10 or 20° resulted in approximately 5 or 10 μm lateral spacing perpendicular to the epoxy-glass interface, yet still maintaining a large space between each indent, roughly 30 μm. This procedure allowed for adequate sampling of the case depth, while placing sufficient distance between each indent. According to the conventions used for indentation,[36,37] the indents should be spaced apart 10–30 times more than the indent depth. In this case, the indent depth was 2 μm; thus, the lower limit of the convention was used because a shorter string of indents made it easier to find a suitable location for indentation along the epoxy-glass interface. The angle between the string of indents and the epoxy-glass interface was set manually; the "zero" was set by visually aligning the epoxy-glass interface of the sample with the internal axes of the indenter actuator.

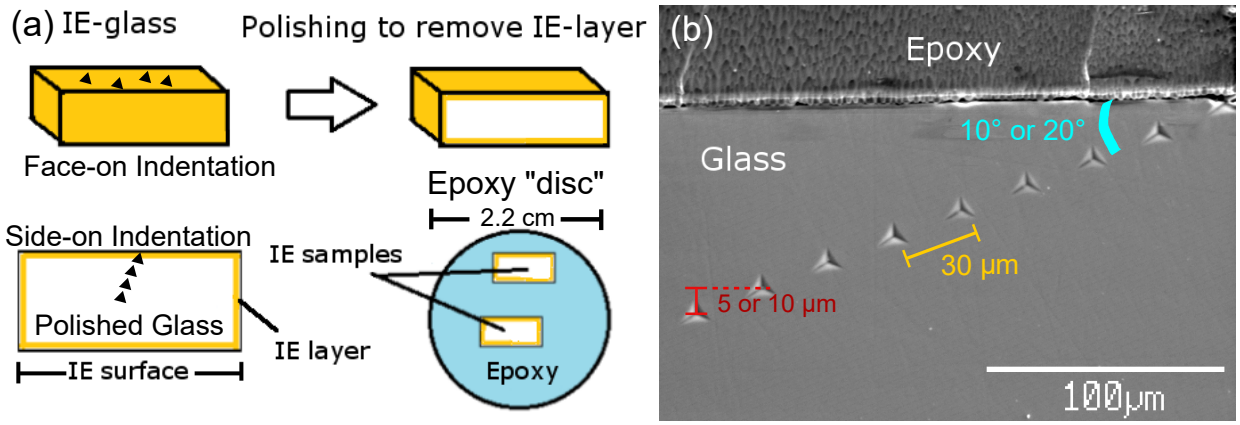

Figure 1: (a) Schematic of removing IE layer and embedding in epoxy disc procedure, along with face-on vs. side-on indentation. (b) An example of the nano-indentation procedure. Image captured using an electron microprobe. The indents were made at an angle, 10 or 20°, to ensure adequate spacing between indents while allowing several indents to be within the IE layer. For a 10 or 20° the lateral spacing between indents was 5.3 or 10.7 μm. The error in the lateral spacing is between 0.1–2 μm as the error compounds with increasing indent number.

Using images collected from WDS and/or an optical microscope, the angle of the string of indents was determined for each IE temperature and was found to be at most $\pm$ 1.5° from the target angle. Although an angle difference of 1.5° is significant over long length scales, it is of less importance nearest the edge where significant changes in mechanical properties are

expected to occur. Nonetheless, the optically *measured* angle values were used to determine the lateral space between each indent. Since the angles were inspected visually, an error of ± 0.25° is estimated, translating to an error range of ± 0.1–2 μm as the error compounds with increasing indent number. Indent images like the one in Fig. 1 also were used to ascertain whether visible pile-up had occurred around the indents.

It was necessary to have the surrounding epoxy upon which to indent, as it was feared indenting near an entirely free edge would negatively affect the indenter. Additionally, it was of paramount importance that all of the indents near the interface be successful; observing the transition from epoxy to glass ensured that the measured mechanical properties were those of the material at the beginning of the case depth. However, indenting continuously from one material to another mechanically different type of material introduced some unique challenges. Firstly, the difference between the mechanical properties of epoxy and glass made it difficult to polish the two materials evenly; finding a continuous straight, clean interface between the epoxy and glass for several indents could be challenging. Additionally, the initial positioning of the indenter tip on the sample needed to be accurate and involved many separate calibrations of the tip's position. Also, due to the mechanics of polishing, it is more likely that the edges of the sample are polished more compared to the sample middle and there is a slope downwards from the middle towards the edge. Although WDS showed the edges to be mostly flat (the technique is sensitive to micron-size changes in height), nano-indentation errors still occurred, presumably caused by elevation differences or "gap" found between the two materials. These issues led to larger uncertainties for indents made near the edge compared to indents made further from the edge of the specimen.

Results

Displacement Plots

Plots of stiffness or hardness vs. displacement into the surface are shown in Fig. 2 for the edge of the sample exchanged at 390 °C. These plots readily show the transition from the surrounding epoxy to the glass sample. For clarification purposes, there are two types of distance being discussed; there is indent depth or displacement into surface, which is between 100–2000 nm, contrasted with lateral distance from the sample edge or case depth, usually between 5–100 μm. In the displacement depth plots of 390 °C (Fig. 2), indents 1 & 2 were made on the epoxy, measuring stiffness and hardness values of ≤ 10 and ≤ 0.25 GPa, respectively. Next, indent 3 shows where the tip first measures the epoxy and then at a larger displacement contacts the glass sample. Conversely, indent 4 in Fig. 2 was on the glass, yet near enough to the interface that the glass is weak and appears to fail at large penetration depths, > 1400 nm.

Continuing with increasing indent number or lateral distance from the edge, indents 5 and 6 demonstrate larger-than-expected Y and H values at low indent depths, 100–600 nm, and then significantly lower Y and H values for larger displacements into the surface, 1500–2000 nm. A downwards slope with increasing indent depth is ISE behaviour, although normal ISE behaviour usually stops above a certain indent depth, after which a displacement-independent value is obtained. In this case, we are observing a sharper slope 100–500 nm and a shallower slope that continues for the entire depth of the indent (500–2000 nm). As mentioned earlier, we do not expect an ISE in IE glasses for indents deeper than 500 nm,[6] so it may be that the steeper slope found between 100–500 nm is the typical ISE, however, without more information, we are calling the behaviour ISE-*like*.

At higher indent numbers (7–9), *i.e.*, further from the edge, hardness no longer shows an ISE-like behaviour, *only* stiffness maintains the downwards slope. WDS analysis showed [K_2O] to be significant in the 25 μm nearest the edge, thus, indents 8 and 9 are likely near the

end of the IE layer. Although they are not shown, indents made past the case depth do not possess this type of behaviour—that is, the Young's modulus and hardness are independent of indent depth (for penetration depths greater than 200 nm) outside of the IE layer. Other IE temperatures (420–480 °C) can be found in the SI. In contrast, Young's modulus as a function of indent depth for the middle of the untreated sample, $30Li_2O$-$70SiO_2$ (see SI), shows a constant stiffness value past an indent depth of 200 nm.

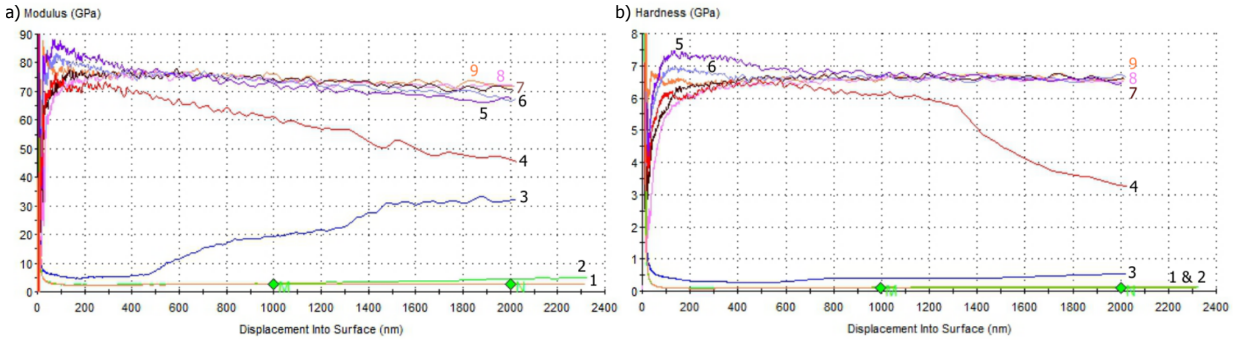

Figure 2: Young's modulus (a) and hardness (b) vs. displacement into surface for the 390 °C IE sample. Indents 1 and 2 were made on the epoxy surrounding the sample, indents 3 and 4 were made on the epoxy-glass interface, and indents 5–9 were made on the glass. Additional plots of Young's modulus and hardness as a function of displacement for each sample are available in the SI.

Although only one displacement plot is shown (Fig. 2) all other IE temperatures were found to show this decrease in Young's modulus and hardness (near the edge *only*) with increasing penetration depth within the IE layer as well. This ISE-like behaviour could be caused by several factors. First, as discussed earlier, nano-indentation assumes that no pile-up of the material occurs around the indent; if pile-up occurs, it has been known to result in erroneously large H values. We can use the empirical rule developed by Pharr,[25] where if the final-to-maximum displacement ratio is less than 0.7 , no pile-up is expected for the indent. Essentially, the lower limit of h_f/h_{max} corresponds to fully elastic behaviour, while the upper limit indicates plastic deformation.[38] Fig. 3 shows the displacement curve for the 390 °C sample, demonstrating that pile-up is expected for indents 3–4, since the final displacement after unloading is more than 0.7 of the maximum displacement, while

pile-up is *not* expected for indents 5–10. The shape of indent 4 is similar to that seen for a multi-layered material with a harder layer on top.[24] This agrees with what was observed in WDS images of the indents; when indents were made completely on the glass no evidence of pile up, however, indents straddling the epoxy-glass interface were seen to have pile-up, even on the glass side. The other IE temperatures, 405–480 °C, showed similar behaviour in the displacement curves and WDS images, thus pile-up is not the reason for ISE-like behaviour when indents are made at least 10 μm from the sample edge.

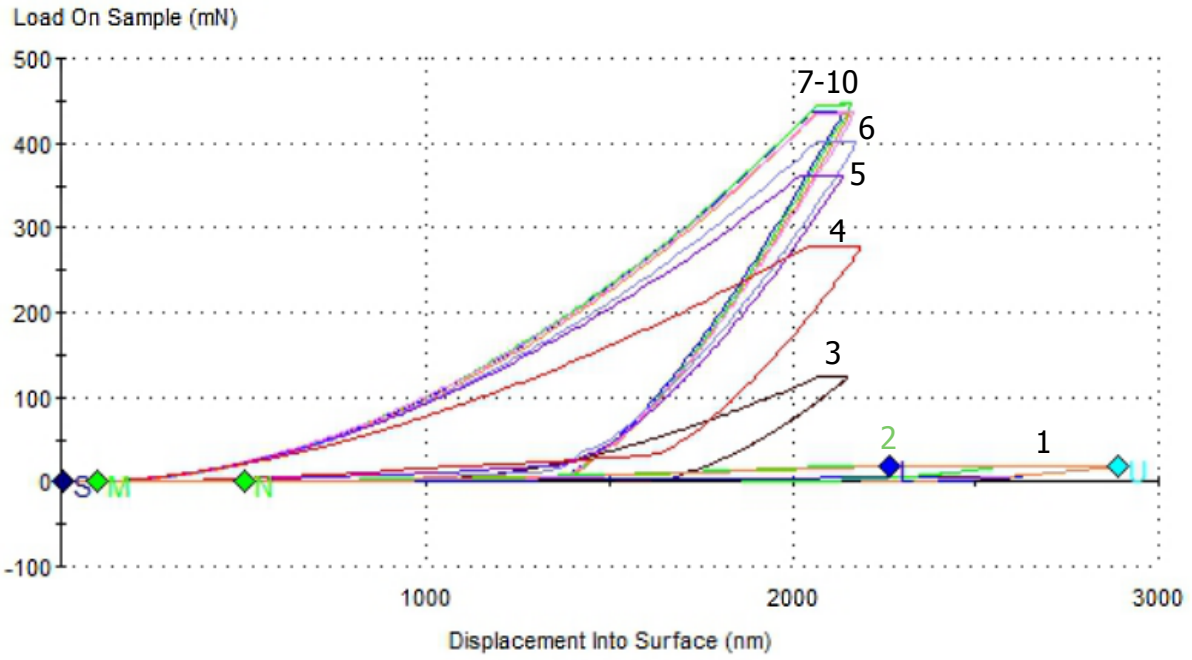

Figure 3: Load-displacement curve produced from nano-indentation for the 390 °C IE sample. Indents 1 and 2 are clearly on the epoxy, while indents 3 and 4 are near the epoxy-glass transition, likely indent 3 is on the epoxy, while indent 4 is on the glass, but near the sample edge ($<$ 10 μm). Indent 5–8 are fully into the case depth of the IE glass, while indents 9–10 are likely past the case depth and into the untreated region of the IE sample (known from WDS results).

Tilting of the indenter tip, which can be caused by an incline of the surface resulting from polishing, can also increase measured Y and H. An example of this is seen clearly for indent 2 (green) in the 480 °C sample (see SI) where based on studies of effects of tip tilting, the tilt can be estimated to be 10°. It is also possible that tilting could occur from the compositional gradient found in the IE glasses resulting in varying degrees of stiffness or

hardness on opposite sides of the indenter tip. However, the ISE-like behaviour is found even when the compositional gradient is small relative to the indent size; elemental analysis from WDS reveals a plateau of fairly constant mixed-alkali composition, approximately $10K_2O$-$20Li_2O$-$70SiO_2$, in the IE glasses over several of 10s of microns. Only the the tail-edge of the diffusion profile is likely to have a steep compositional gradient. Finally, the micrographs also show the indents to be symmetric, not asymmetric as would be expected from a tilted indent. Consequently, we do not believe the ISE-like behaviour in the IE layer could be a result of the compositional gradient. Nonetheless, since it is possible that the sample is sloped at the edge from polishing and there was piling up observed around indents made along the epoxy-glass interface, a possible error of 6–10% was estimated for the Y and H data measured within 20 μm of the sample edge (as seen in the following case depth plots).

Case Depth Dependence

Since samples exchanged at all IE temperatures displayed ISE-like behaviour far enough from the sample edge where no pile-up or incline from polishing was expected, the mechanical properties were evaluated over two indent depth ranges: a shallow (150–300 nm) and a deep (1500–2000 nm) displacement. The indent shape is the same for both displacements, only the depth range over which the mechanical values are averaged is different. Fig. 4 shows the stiffness as a function of case depth for a deep indent; each data point is a different indent further from the edge of the sample and the penetration into the surface of each indent is deep (1500–2000 nm). The "zero" was set for each IE temperature at the beginning of the sharp increase in stiffness, however, due to sampling resolution, the actual epoxy-glass interface may be shifted 2–5 μm to the right.

First of all, the stiffness of the untreated ($30Li_2O$-$70SiO_2$) composition (70 GPa) matches the value measured ultrasonically for the bulk sample (75 GPa). Valid nano-indentation is reported to have an accuracy of better than 10% when compared to bulk values.[39] Strikingly, the untreated sample is much more compliant in the 30 μm nearest the sample edge.

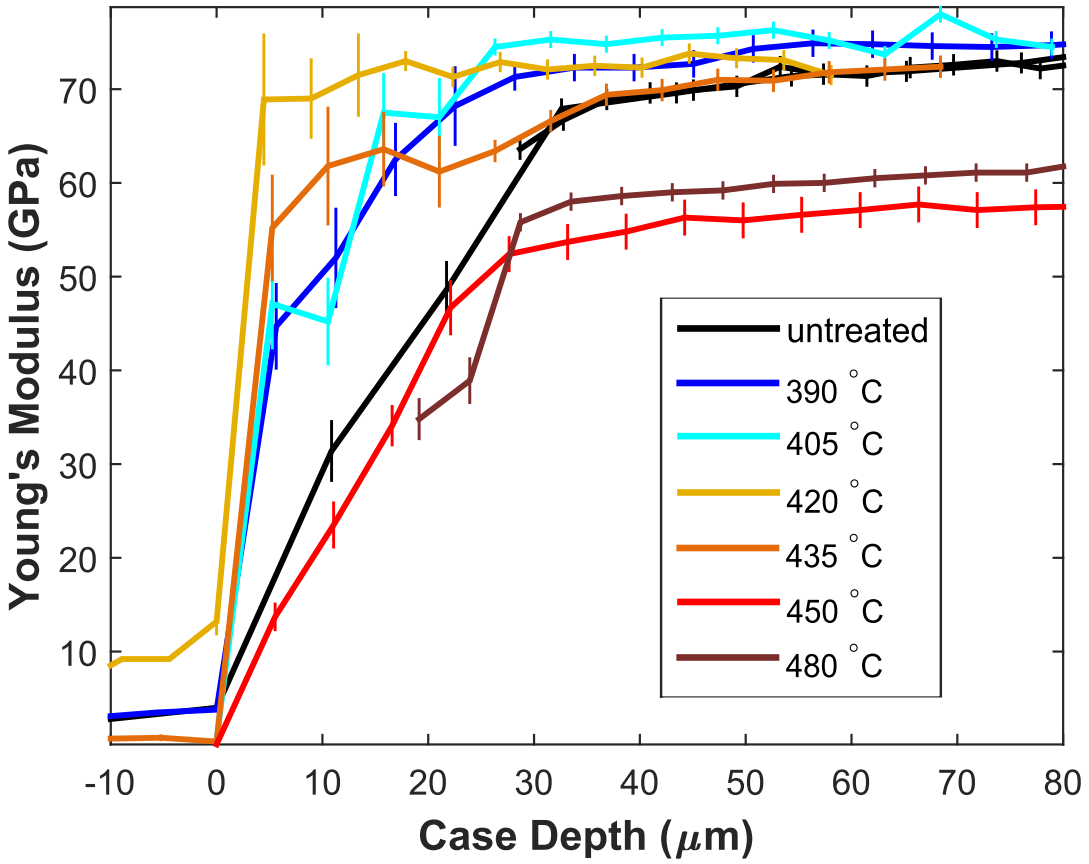

Figure 4: Comparison of the Young's modulus for all IE temperatures, 390–480 °C (dark blue–dark red) with two untreated (black) lithium silicate glasses, at a *deep* displacement depth of 1500–2000 nm.

This is likely because there are fewer constraints, such as bonding to the rest of the bulk material, at the edge. Several studies have examined nano-indentation near an interface or free edge;[40–43] they found that the material's mechanical properties were somewhere between those of the two phases. For example, indenting a polymer matrix near a glass fibre leads to increased apparent elastic modulus, while indenting the same polymer near a free edge caused a decrease in apparent elastic modulus.[42] More importantly, the stiffness and hardness of fused silica were seen to decrease linearly when indented near a free edge.[40] Although we are indenting glass near epoxy, the large disparity in mechanical properties between glass and epoxy is similar to a free edge.

Jakes et al.[40] attributed the lower Y to an additional effect called *structural compliance*, which is negatively correlated with distance from the sample edge while being independent of the depth of the indent. When the material is more compliant and plastic (as will be shown), it is possible that the assumptions which are integral to determining mechanical properties from nano-indentation may break down since they presume an elastic response. However, Jakes et al. used atomic force microscopy to image the indents, thereby, proving the material is less stiff and hard near an edge—it is not an artifact of the continuous depth-sensing analysis.

Low IE temperatures, 390–405 °C, enhance the stiffness near the edge (0–30 μm) and even have higher Young's moduli in comparison to the untreated sample beyond that first 30 μm (Fig. 4). This second result is somewhat surprising for the 390 and 405 °C samples, since the stiffness is enhanced past the depth of the IE layer as determined by WDS. Possibly the additional thermal treatment for 72 hours led to densification and increased Y.

The sample exchanged at 420 °C shows the most complex behaviour; it has the most improved stiffness nearest the edge, but then appears to rejoin the Young's modulus of the untreated sample around 55 μm (approximately where the IE layer ends). The sample exchanged at 435 °C shows a very similar behaviour, only with less enhancement near the edge. It is somewhat surprising that samples exchanged at these middle IE temperatures,

420 and 435 °C, appear to be returning to the baseline Young's modulus of the untreated sample, when both of these samples are in fact mixed-alkali within the case depth for the data shown. They do not have the Y expected for an as-melted mixed-alkali composition, as Y was observed to decrease with the addition of K_2O in the bulk Li_2O-K_2O-SiO_2 series. Instead these IE temperatures appear to have similar stiffnesses to the starting material, 30%Li_2O, perhaps indicating some, but incomplete relaxation of the compressive stresses due to thermal treatments near, but still below T_g (465 °C).

Finally, samples exchanged at 450 and 480 °C demonstrate the result of significant thermal relaxation—that is, there is no improved Y near the edge and the final Young's modulus is well below that found for the untreated sample. In fact, the stiffness for these two samples, 55–60 GPa, is lower than expected from the measurements on the compositionally equivalent bulk glass, 72 GPa. In part, this discrepancy may be due to heating the glass well-above its initial fictive temperature ($T_f \approx 415$ °C). Additionally, cracking was observed between the indents in the sample exchanged at 450 °C, which may contribute to it having *lower* stiffness than the sample exchanged at 480 °C.

The stiffness as a function of case depth averaged over a shallow indent range (150-300 nm) is shown in Fig. 5. The trends are very similar as those seen for the deep indent data (Fig. 4), albeit somewhat noisier. IE temperatures well-below T_g, 390–435 °C, show enhanced stiffness near the edge in comparison with the untreated sample, while samples exchanged at high temperatures, 450 and 480 °C have stiffnesses below that of the untreated material (as expected for the corresponding as-melted mixed-alkali compositions). The main difference is that *all* samples, even the untreated composition, are much stiffer near the edge (first 30 μm) at shallow indent depths. Additionally, the stiffness values measured here are 13–40% higher than those averaged over deep displacements, demonstrating the ISE-like behaviour seen in the displacement plots in Fig. 2. Finally, samples exchanged at low temperatures, such as 390 and 420 °C, have high stiffnesses near the edge (0–15 μm), perhaps indicating more pronounced ISE-like behaviour in this region, in addition to agreeing with the results

from face-on nano-indentation (Table 1).

Table 1 also contains the hardnesses from micro-indentation for the untreated and IE samples. As expected, IE improved the mechanical properties, however, the trends in hardness are different whether nano- or micro-indentation was used. In comparison with the untreated sample, IE temperature 390 °C shows increased hardness during face-on nano-indentation, yet a decrease in H when micro-indentation is performed. Conversely, the sample exchanged at 420 °C shows the opposite trend; nano-indentation indicates a degraded hardness, while micro-indentation shows improved H. Both indentation techniques begin to measure decreased stiffness and hardness at high IE temperatures, 435–450 °C.

Table 1: Average Y and H from face-on (before removal of IE layer) nano-indentation of the middle of the sample in comparison to H from micro-indentation

Sample	Y (GPa)	H (GPa) (nano)	H (GPa) (micro)
untreated	74.9(5)	6.65(5)	5.2(1)
390 °C	78.9(4)	6.91(4)	5.07(6)
405 °C			5.4(1)
420 °C	77.0(8)	6.0(1)	5.25(8)
435 °C			5.1(1)
450 °C	67.7(9)	5.2(1)	

Fig. 6 displays the hardness as a function of case depth averaged over a deep displacement (1500-2000 nm). In this case, the "zeroes" were set from the Y data in Fig. 4, thus, we can compare the stiffness and hardness data at the same case depth since they come from the same indent. As expected, the untreated composition is softer near the edge (0–30 μm) than at the middle of the sample. The nano-hardness of the 30% Li_2O sample is significantly higher than what was found by micro-indentation of the bulk composition, 6.5 vs. 5.2 GPa. Although this is a large discrepancy (25%), the load is known to greatly affect the hardness values obtained due to the ISE.[26] In fact, nano- vs. micro-indentation has been seen to have a difference of 22% for IE glasses,[6] and 10–440% for other materials.[44,45]

In terms of the effect of IE temperature, the hardness data have strikingly similar trends to the stiffness data; the low IE temperatures (390 and 405 °C) are harder near the edge

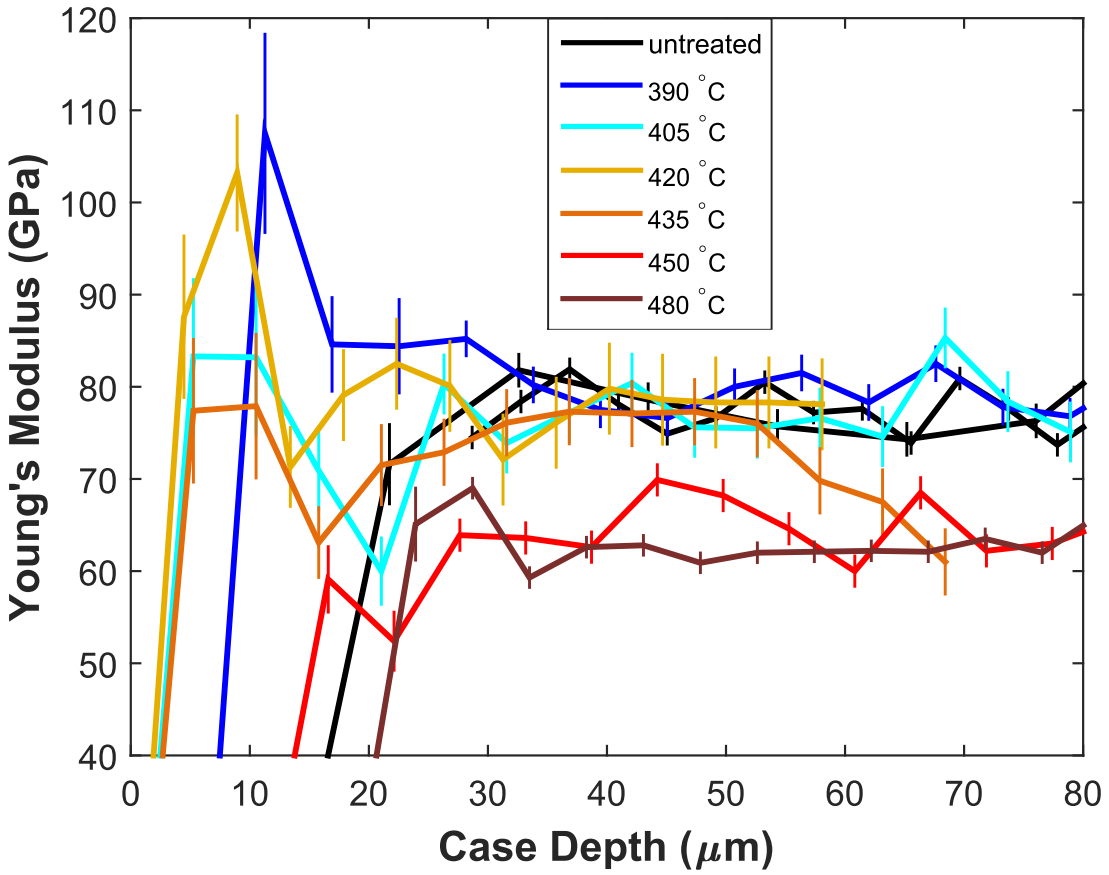

Figure 5: Comparison of the Young's modulus for all IE temperatures, 390–480 °C (dark blue–dark red) with two untreated (black) lithium silicate glass samples, at a *shallow* displacement depth of 150–300 nm.

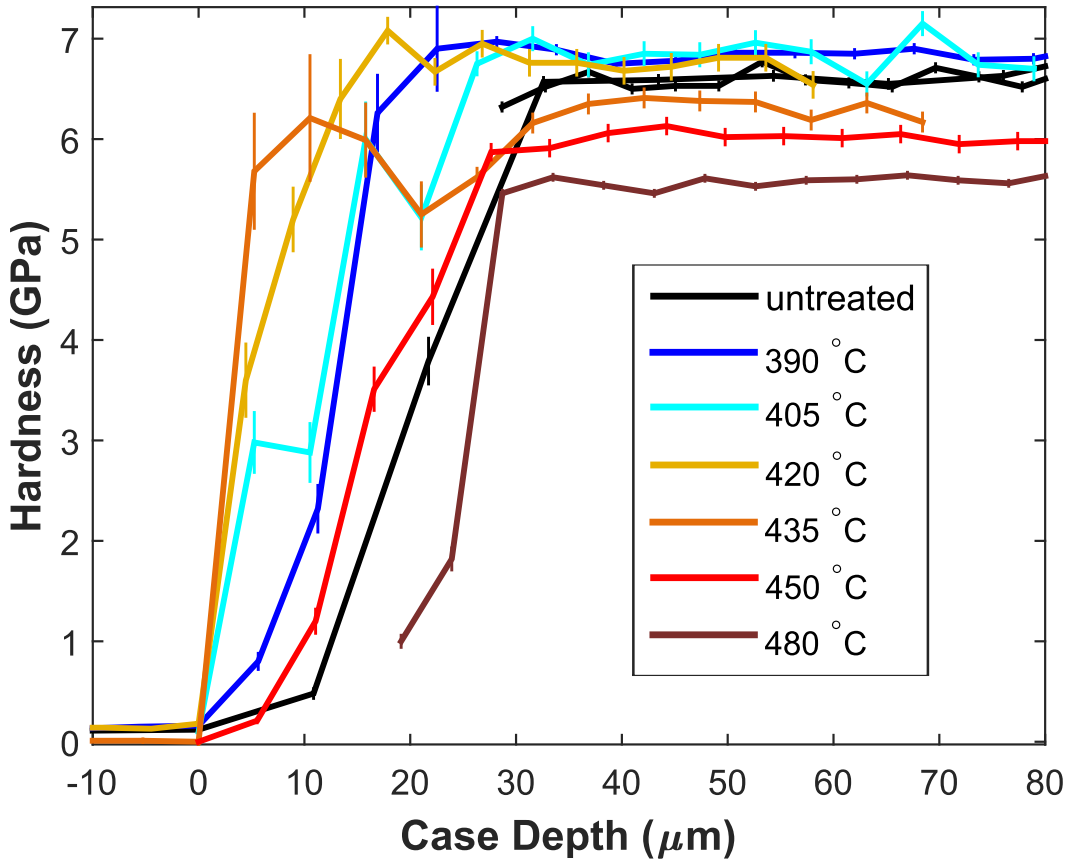

Figure 6: Comparison of the hardness for all IE temperatures, 390–480 °C (dark blue–dark red) with two untreated (black) lithium silicate glass samples, at a *deep* displacement depth of 1500–2000 nm.

and beyond the case depth, the middle IE temperatures (420 and 435 °C) offer enhanced hardness near the edge *only*), while the high IE temperatures (450 and 480 °C) are thermally relaxed ($T >> T_f$) and have lower hardness throughout their case depths, as was observed by Svenson et al..[7] The notable differences are that the 435 °C sample has higher hardness near the edge, yet lower hardness further into the case depth, both in comparison to the hardness of the untreated composition. Additionally, as expected the 480 °C sample is softer than the 450 °C sample. It appears that an IE temperature of 420 °C is a turning point, after which the hardness decreases predictably with increasing IE temperature. Based on the composition profiles from WDS, the case depth where the hardness of IE samples matches the untreated is approximately where the IE layer ends without the lag observed in the Young's moduli measurements in Fig. 4

The hardness data as function of case depth averaged over a *shallow* indent depth (150–300 nm) is shown in Fig. 7. Temperatures below T_g (459 °C) where significant IE occurred, 390–435 °C, show increased hardness compared to the untreated sample *near the edge*, however, the hardnesses decrease with increasing case depth until they are approximately equal to the untreated value. Conversely, temperatures near or above T_g, 450 and 480 °C, show decreased hardness compared to the untreated sample throughout the case depth. Additionally, the low-temperature IE sample (390 °C) has the largest increase in hardness which agrees with the results from nano-indentation done perpendicular to the IE layer (Table 1).

Normalization

To quantify the improvement in mechanical properties induced by IE, the data were normalized with respect to the untreated composition, Y/Y_0 and H/H_0, and is plotted in Figs. 8 and 9, respectively.

These figures demonstrate the improvement of stiffness and hardness compared to the untreated composition at the same case depth. First, all of the improvement is in the first

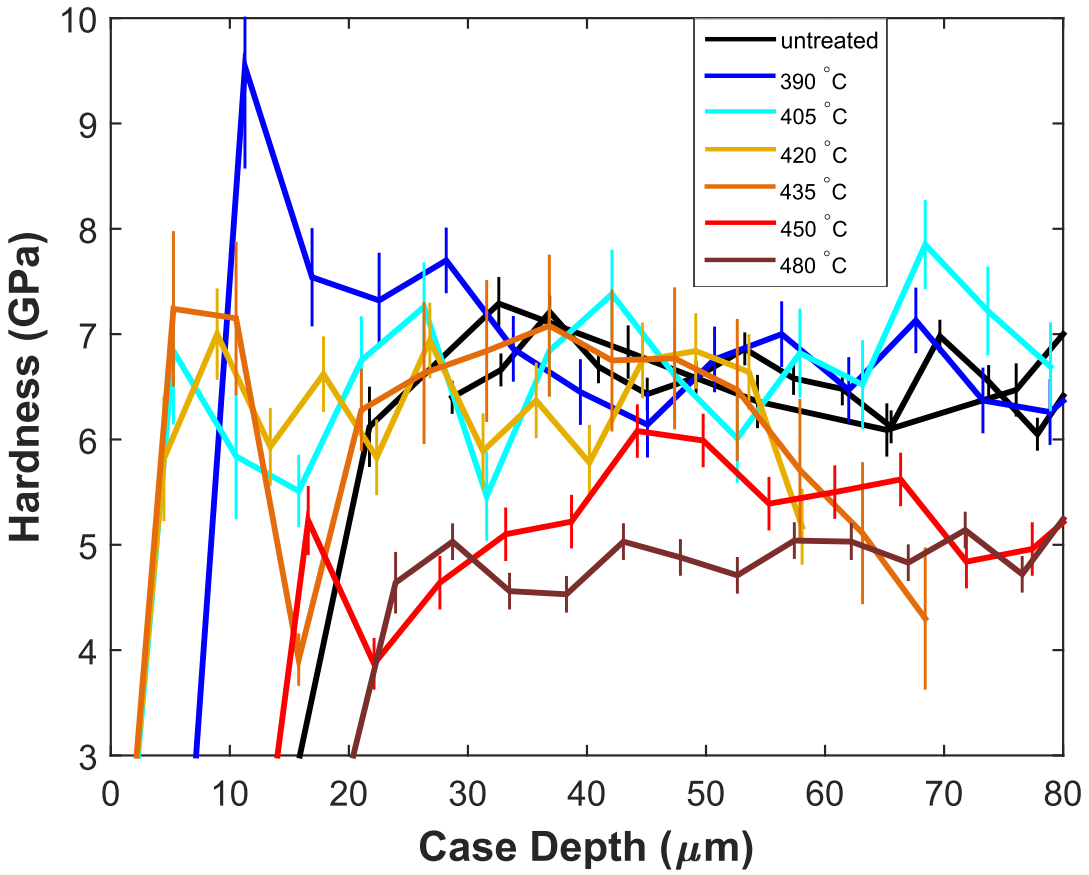

Figure 7: Comparison of the hardness for all IE temperatures, 390–480 °C (dark blue–dark red) with two untreated (black) lithium silicate glass samples, at a *shallow* displacement depth of 150–300 nm.

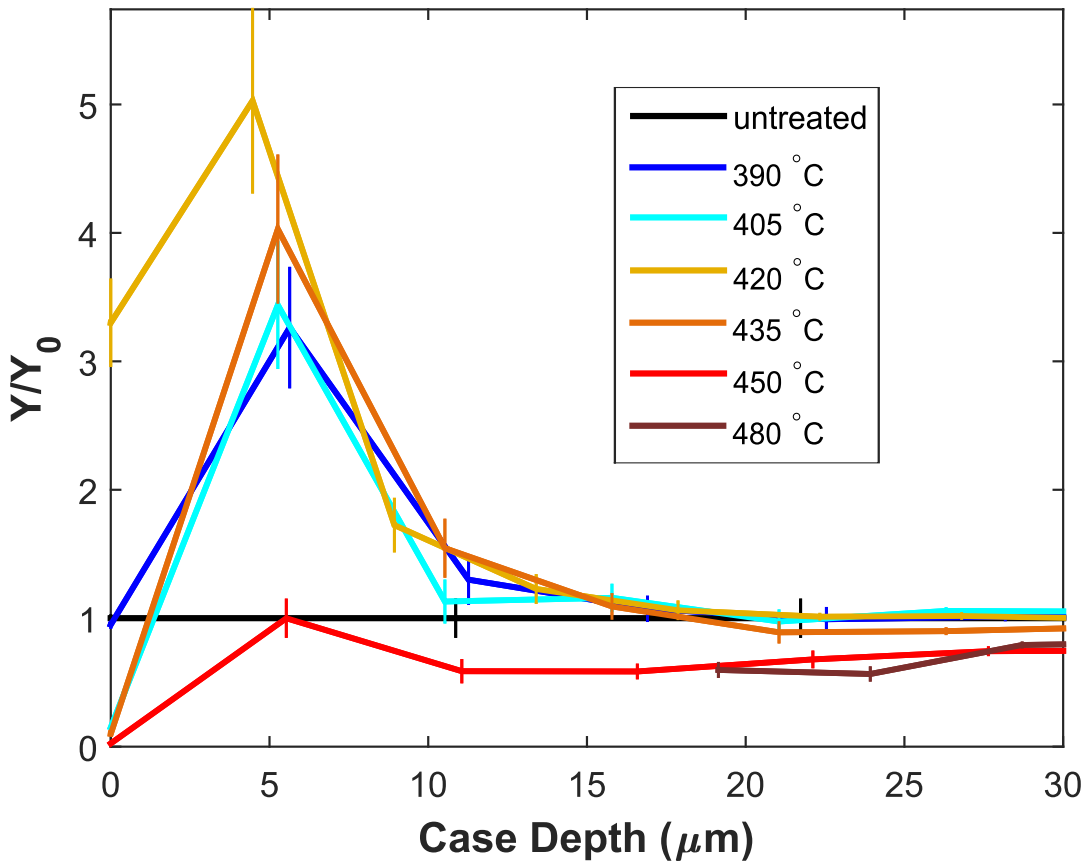

Figure 8: Improvement in Young's modulus in comparison to the untreated lithium silicate glass (Y/Y_0) as a function of case depth for all IE temperatures, 390–480 °C (dark blue–dark red). Only deep indent data (1500–2000 nm) were used. Values above unity indicate enhancement, such as for IE temperatures below T_g (459 °C) where significant IE occurred, 390–435 °C, while high IE temperatures, 450 and 480 °C, saw significant thermal relaxation and have values below one, signifying decreased stiffness.

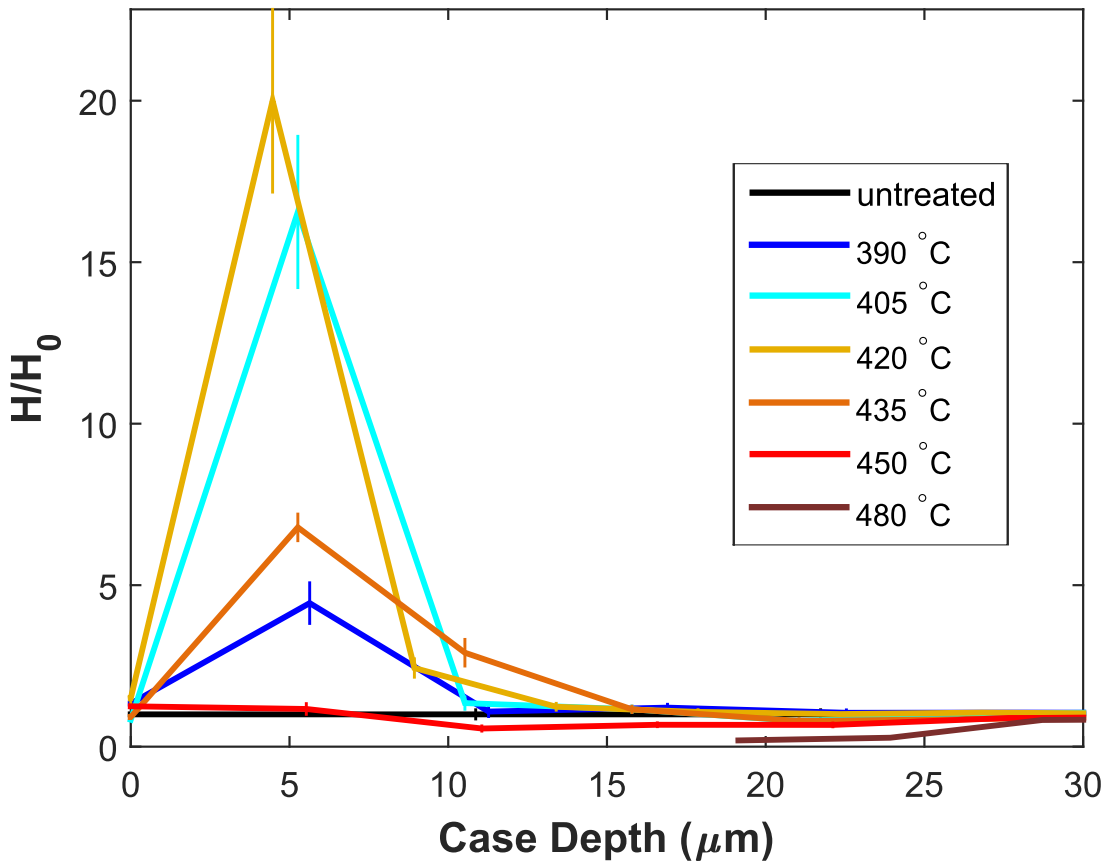

Figure 9: Improvement in hardness in comparison to the untreated lithium silicate glass (H/H_0) as a function of case depth for all IE temperatures, 390–480 °C (dark blue–dark red). Only deep indent data (1500–2000 nm) were used. Values above unity indicate enhancement, such as for IE temperatures below T_g (459 °C) where significant IE occurred, 390–435 °C, while high IE temperatures, 450 and 480 °C, saw significant thermal relaxation and have values below one, signifying reduced hardness.

25 μm nearest the edge. Secondly, IE temperatures below T_g where compressive stress is expected (390–435 °C) have normalized mechanical properties greater than unity, while high IE temperatures (450 and 480 °C) have Y/Y_0 and H/H_0 values below unity, indicating degraded mechanical properties. Both of these observations are expected from the deep indent data in Figs. 4 and 6, however, the normalization plots clearly indicate that hardness has improved vastly in comparison to the stiffness near the sample edge. Hardness was seen to improve 5–20 times, while stiffness has only a 3–5 fold enhancement compared to the mechanical properties of the untreated composition.

Discussion

Generally, the IE process appears to negate the free edge effect, *i.e.*, Y and H near the edge approach similar values to those found in the middle of the untreated composition. IE at 420 °C gives the most enhancement in Y near the immediate edge, however, the low IE temperatures 390 and 405 °C result in higher Y values further into the case depth (Fig. 4). It is possible that the improvements in stiffness are due to high compressive stresses found at low thermal treatments and possible crack healing known to occur as a result.[46] For an industrial piece of float-glass, cracks are typically on the order of 10 μm in depth.[5] Thus, based on Griffith's work,[4] we would expect the sample exchanged at 420 °C to arrest cracks at higher stresses, *i.e.*, be stronger, than the other IE samples. However, the IE temperatures 390 and 405 °C result in higher Y after the first 10 μm, thus, they would likely arrest deeper cracks most effectively. However, the trends seen for Y in Figs. 4 and 8 are different from those observed in compressive stress.[7,14] In a separate experiment micro-Raman spectroscopy was used to determine that IE temperature 390 °C has the highest compressive stress, while the 405 and 420 °C samples have lower compressive stresses spread over a wider case depth.

Although bulk modulus (volumetric stiffness) depends linearly on pressure,[22] it is not immediately clear how the uniaxial stiffness will behave; for a brittle material, it is difficult

to measure the changes in Y as a function of pressure. As a result, nanoindentation of IE glass actually offers a unique example of measuring the effect of compression on Y. Young's moduli of borates and borosilicates show a strong dependence on isostatic pressure, increasing by 10% with only 500 MPa of applied pressure.[47] However, even at low pressures, borates are known to undergo a structural change from BO_3 to BO_4 units[48] leading to a more constrained network and increased rigidity.[49] On the other hand, no significant structural transformation is expected in SiO_2, as no permanent densification was observed for pressures up to approximately 10 and 2 GPa for pure silica and $10Na_2O$-$90SiO_2$, respectively.[50]

However, it is important to recognize compressive stress is not expected to change the stiffness greatly; for most materials, the bulk modulus (K) has only a small dependence on pressure (P), where $K(P) = K(0) + 4P$ (for isostatic stress, $\sigma = 3P$).[22] Thus, if there were an axial stress of 500 MPa in the IE glass, an increase of only 2 GPa would be expected in K. Assuming that Poisson's ratio (ν) remains approximately constant under compression, this translates to an increase of only 3 GPa for Y. However, the deep indent plots of Y and H show enhancements of 20–40 GPa near the edge (0–30 μm) and 5–8 GPa further into the case depth. It is important to remember there are also compositional effects from the MAE occurring in these glasses; a mixed Na-Li silicate system was seen to increase Y up to 36% in comparison to the single alkali end-member.[21] Although compression may be affecting the stiffness, the MAE likely plays a larger role.

Evaluating hardness, the 405 and 420 °C samples are the most improved near the immediate edge (0–10 μm), however, the samples exchanged at 390–405 °C have higher hardnesses further into the case depth. Once more these results do not align with the trends found for face-on nano-indentation and compressive stress; we would expect the 390 °C sample to have the highest hardness especially near the edge. This disagreement is more surprising for hardness, as it is expected to strongly depend on compressive stress. Indentation hardness involves plastic deformation in directions perpendicular to the load, therefore, shear stresses (which has both compressive and tensile components) must occur. Consequently,

compressive stress increases hardness simply by forcing the tensile stresses to first overcome the opposing compressive stress *before* deforming permanently. However, the MAE is known to limit ion mobility and improve the hardness compared to the single-alkali end member, even more than the stiffness (47%).[21] Thus, compositional effects could be responsible for some of the observed enhancement as well as the differences between trends in Fig. 9 versus compressive stress.

Comparing the results when nano-indentation was performed perpendicular to the case depth (Table 1) versus when it was performed along the cross-section (Figs. 4 and 6), the sample exchanged at 390 °C showed similar improvements in both cases, while the 420 °C sample did not. IE temperature 420 °C saw improvements in both stiffness and hardness in the side-on case, yet face-on measurements showed only Y to be higher, while H was actually lower than the untreated sample. Furthermore, the IE temperature 450 °C sample has a much lower hardness for face-on measurements in comparison to the side-on values. These differences may be a matter of position and scale; the face-on measurements are made far from a free edge and only probe the topmost 2 μm Relaxation is known to occur at the immediate edge,[5,14] thus high IE temperatures likely have relaxation occurring in the few topmost microns that the cross-section view does not observe. Nonetheless, it is interesting that hardness appears to be more affected by relaxation at the immediate edge in comparison to stiffness. This result agrees with the above idea that stiffness is more affected by composition and the resulting MAE in comparison with hardness which depends heavily on compressive stress.

The micro-indentation results in Table 1 show a different trend, where the hardness decreases for the sample exchanged at 390 °C likely because the resulting indent was deeper than the IE layer, leading to worse mechanical properties due to the mixed composition within the layer as well as the tensile stress expected beyond the IE layer. On the other hand, IE temperature samples 405 and 420 °C saw enhanced hardness due to a thicker IE layer relative to indent size. Overall, the results from nano-indentation of the cross-section (nor-

malized hardness in Fig. 9) agree well with the hardness trends found for micro-indentation; samples exchanged at 405 and 420 °C have the most improved hardness in comparison with the untreated composition. This demonstrates how the improved hardness observed in the first 10 μm of the IE layer, a relatively small volume, is a predictor of the micro-mechanical behaviour of the material. In contrast, the 390 and 435 °C samples saw improvement in nano-hardness, yet not in the micro-hardness measurements. This disagreement is likely due to the difference in size of indents, where the low cumulative compressive stress was overcome by micro-indentation, but not nano-indentation. This demonstrates how the indentation process damages the material, thereby relaxing the compressive stress as penetration occurs, leading to results that are dependent on indent penetration depth as corroborated by the displacement plots (Fig. 2) and following section.

Given that the side-on nano-indentation procedure yielded hardness trends that matched those of the micro-hardness experiments, it may be supposed that the nano-indentation trends for Y are also valid on the micron scale. This is interesting because it is generally difficult to probe the mechanical properties, especially Young's modulus, of a thin layer such as the IE case depth. Thus far, studies have only performed face-on nano-indentation perpendicular to the case-depth,[6] which we show here to not accurately reflect the material's micron-scale behaviour. Consequently, the behaviour of Y shown here can be used in mechanical modelling of the IE layer, such as in the case of the determination of the linear network dilation coefficient (LNDC) which has been shown to correlate negatively with Y.[14] Generally, Y has been considered to be invariant with compression within the IE layer, which is a reasonable assumption sufficiently far from the free edge (> 30 μm); Y only increases about 6% past this case depth. Nonetheless, the free edge effect causes significant decreases in stiffness near the edge and should be taken into consideration when modelling surfaces. However, it is worth noting that near the free edge, a constant Y is a *more* valid assumption for IE glasses than it is for an untreated sample as IE appears to negate most of the free edge effect.

ISE-like Behaviour

In order to better evaluate the ISE-like anomaly, its magnitude was quantified by comparing the Y and H values evaluated over shallow indent displacements to the corresponding values at deep indent displacements. Fig. 10 plots the stiffness value averaged over a shallow indent depth (150–300 nm) divided by the stiffness value averaged over a deep indent range (1500-2000 nm), $Y_{\text{shallow}}/Y_{\text{deep}}$. These values come from the *same* indent, the stiffness is being averaged at different indent depth ranges only.

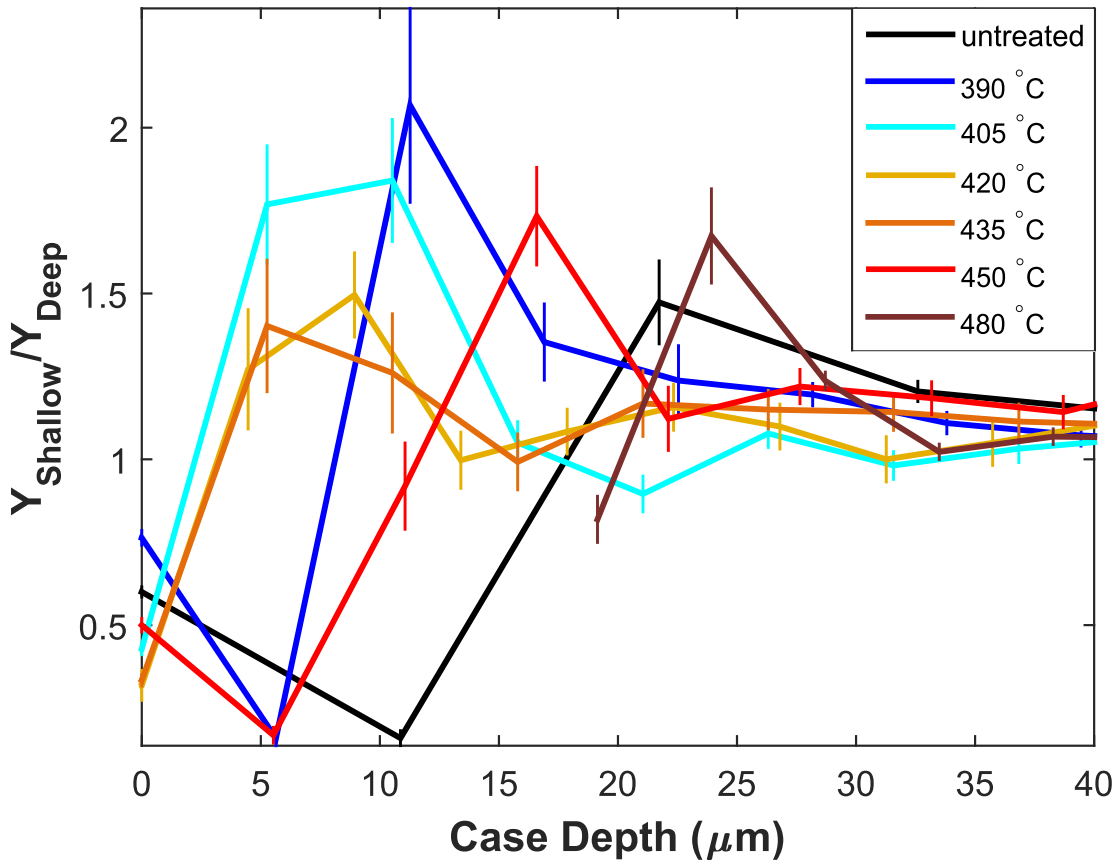

Figure 10: Evaluation of the ISE in Young's modulus by comparing values averaged over shallow vs. deep indent displacements ($Y_{\text{shallow}}/Y_{\text{deep}}$) as a function of case depth for all IE temperatures, 390–480 °C (dark blue–dark red) with the untreated (black) lithium silicate glass. Values above unity indicate a ISE-like behaviour, while values below one, signify a reverse ISE-like behaviour, where the stiffness is lower at shallow indent depths.

In Fig. 10, unity represents the absence of ISE-like behaviour; the stiffness measured

at shallow indents depths is the same as for deep indent displacements. All IE temperatures have little to no ISE ($Y_{\text{shallow}}/Y_{\text{deep}}$ of approximately 1–1.15) for case depths greater than 40 μm, which is smaller than those reported for fused silica (1.25[33]) and bulk metallic glasses (1.4[30]) alike. When $Y_{\text{shallow}}/Y_{\text{deep}}$ is greater than unity, it is indicative of ISE-like behaviour—the material is stiffer at shallow displacements, while a value below zero represents a behaviour sometimes referred to as reverse ISE-like behaviour[26]—the material is more compliant at shallow displacements. As a reminder, the "zero" position is the same one used in the plot of stiffness vs. case depth in Fig. 4.

Perhaps one of the most interesting observations about Fig. 10 is that the untreated sample itself shows complex behaviour near the edge of the sample, ≤ 30 μm. This indicates that ISE-like behaviour may be inherent to measurements made near the sample edge, which as discussed earlier could be caused by tip tilting due to inclines near the edge. If that is the case, hardness is expected to be more affected by sample tilt compared with stiffness. Fig. 11 shows the same type of shallow vs. deep indent plot, but for hardness ($H_{\text{shallow}}/H_{\text{deep}}$). Comparing the ISE-like behaviour of stiffness and hardness (Figs. 10 and 11), we see that the values and trends are almost identical for all IE temperatures except 390 and 480 °C. Interestingly, those IE temperatures do have the expected dependence for Y and H *if* tip tilting occurred. For example, 390 °C has a $H_{\text{shallow}}/H_{\text{deep}}$ of 4 and a $Y_{\text{shallow}}/Y_{\text{deep}}$ of 2, while 480 °C has a $H_{\text{shallow}}/H_{\text{deep}}$ of 2.5 and a $Y_{\text{shallow}}/Y_{\text{deep}}$ of 1.6. As a consequence, those samples are likely experiencing tip tilting, either as a result of sloping near the edge or a compositional gradient, as discussed earlier. Nonetheless, it demonstrates that the complex behaviours of the untreated and other IE temperature samples are likely due to another physical phenomenon.

Although a complex behaviour such as the one exhibited by the untreated sample is rarely observed in an amorphous, isotropic material such as glass, it is important to realize that the ISE has been shown to be very sensitive to the surface condition.[26] There have been several articles on the difficulties and importance in preparing a flawless surface for

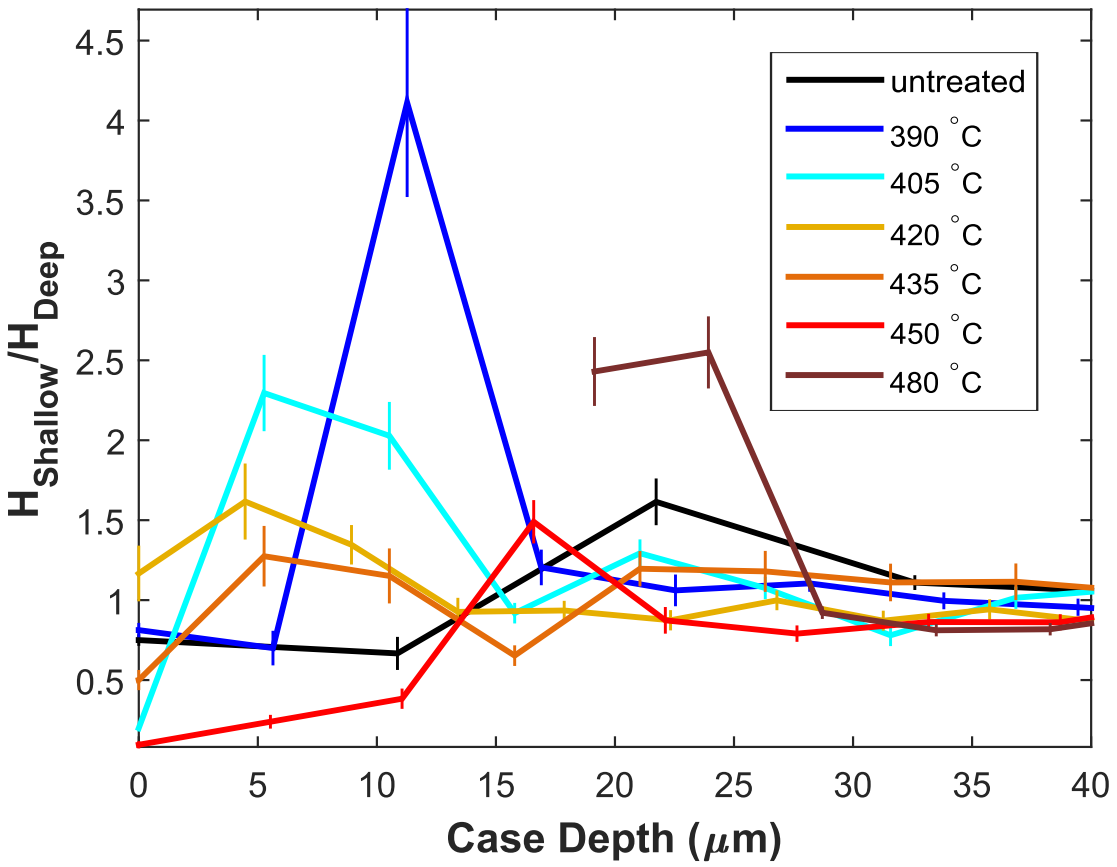

Figure 11: Evaluation of the ISE in hardness by comparing values averaged over shallow vs. deep indent displacements ($H_{\text{shallow}}/H_{\text{deep}}$) as a function of case depth for all IE temperatures, 390–480 °C (dark blue–dark red) with the untreated (black) lithium silicate glass. Values above unity indicate a ISE-like behaviour, while values below one, signify a reverse ISE-like behaviour, where the hardness is lower at shallow indent depths.

nano-indentation.[51–54] In fact, when a single crystal of Cu was polished in two different manners (colloidal silica vs. electropolishing) the magnitude of the ISE was seen to reduce significantly;[52] using our notation here, the $H_{\text{shallow}}/H_{\text{deep}}$ decreased from 1.7 to 1.2 because of surface preparation technique alone. As a consequence, it may be less surprising that the untreated sample shows ISE-like behaviour near the edge, where surface flaws are present. Additionally, since stiffness and hardness are known to decrease near a free edge,[40] it may simply be that the geometry of the indenter is such that a deeper indent probes closer to the material's edge.

Although it is interesting to attempt to understand the reason why ISE-like behaviour is occurring near the edge in all samples, the answer lies out of the scope of this investigation. The origins of the ISE are not fully understood for bulk amorphous materials; here we have the added complexity of examining the behaviour of the surface under compression. Not only does the surface condition change under compression, but the compressive stress profile may be changing as the indenter tip displaces the material, thereby affecting the values of Y and H measured at different indent depths. This is indicated by the differences observed between the side-view nano-hardness (Fig. 9) and micro-hardness (Table 1) results. In this study, the behaviour of the untreated sample serves as a baseline to observe the effect of the IE on the mechanical properties at the edge.

Considering $Y_{\text{shallow}}/Y_{\text{deep}}$ for the untreated sample in Fig. 10, it shows reverse ISE-like behaviour very close to the edge, first 10 μm, followed by a positive ISE-like behaviour peak, before going to unity. The lowest IE temperature, 390 °C, has a migration of the "zig-zag" towards the edge, where IE temperatures 405–435 °C immediately have ISE-like behaviour (positive values) at the edge and then at high IE temperatures, 450 and 480 °C, the zig-zag migrates away from the edge and back towards the untreated sample. The most thermally relaxed IE temperature (480 °C) shows nearly the same behaviour within the case depth as the untreated composition. The same migration with increasing IE temperature occurs in the $H_{\text{shallow}}/H_{\text{deep}}$ plot in Fig. 11, although the zig-zag itself tends to be less pronounced for

hardness. Additionally, the ISE-like behaviour persists further into the case depth for the stiffness in comparison to the hardness for most IE temperatures, which agrees with what was observed in the displacement plots in the Results section.

The migration of the ISE peak towards the sample edge in both Y and H may indicate that IE is having a significant effect on the surface condition. For IE temperatures where significant exchange occurring while still being below T_g (405–435°C), the immediate ISE-like behaviour at the edge is likely due to the compressive stress at the edge. In addition to mitigating the concentrated tensile stress at crack tips and arresting crack propagation, compressive stress has been known to promote crack closure, which depending on the extent of closure also leads to significant strengthening.[46] The low IE temperatures, 390 and 405 °C, have the largest values (although some of the height in the 390 °C sample in the $H_{\text{shallow}}/H_{\text{deep}}$ plot may be from another physical process), perhaps indicating that compressive stress leads to larger changes at the surface and more pronounced ISE-like behaviour near the edge. Concurrently, the indenter tip may release compressive stress, *i.e.*, microcracking, as it displaces material. Finally, the peak for the high IE temperatures (450 and 480 °C) in Figs. 10 and 11 migrates back towards the untreated zigzag, demonstrating as the structure relaxes and compressive stress decreases to zero, the same indentation behaviour and surface condition reappear; the role of the surface in the indentation behaviour is the same for a completely relaxed composition, the untreated or 480 °C sample.

Elasticity and Plasticity

One of the goals of this study was to ascertain which mechanical response, elastic or plastic, is more enhanced from the IE process; stiffness is a measure of the elastic response solely, while hardness contains both elastic and plastic components. Although the exact proportions of elastic and plastic resistance to deformation are unknown for these samples, we expect glass to respond mostly elastically, 84% compared with only 14% plastic response.[19] As a result, if the improvement is elastic in nature, *i.e.*, increase in bond density and/or strength, we would

expect the stiffness and hardness to increases similarly after the IE process. Conversely, if resistance to plastic deformation increases, we would expect the hardness to be enhanced more than the stiffness. The previous two normalization plots, Figs. 8 and 9 display clearly that H has a much greater enhancement, indicating that IE increases resistance to plasticity to a greater degree than elasticity.

However, Y or H alone do not fully characterize a material's mechanical response; in fact, the ratio of the two properties (H/Y^*, where $Y^* = Y/(1-\nu^2)$ and ν is the same Poisson's ratio value that was used to convert Y^* to Y in the nano-indentation procedure) has been found to better predict elastic vs. plastic behaviour.[55] According to Musil et al.'s nano-indentation of superhard coatings, H/Y^* is approximately proportional to elastic recovery (ω_e), while H^3/Y^{*2} is correlated with resistance to plastic deformation.[56–58]

Fig. 12 displays the effect of IE temperature on elastic recovery or H/Y^*. It can be seen that for all IE temperatures, with the exception of 480 °C, IE improved the elastic recovery near the edge (0–30 μm) compared to the untreated composition. Interestingly, past 30 μm of case depth none of the IE temperatures lowered the elastic recovery (H/Y^*) in comparison to the untreated sample, despite both of the samples exchanged at 450 and 480 °C having lower Y and H in that region. Initially, an increase in IE temperature enhances elastic recovery closer to the immediate edge until the sample exchanged at 420 °C, which has the most improved elastic response closest to the edge. Thereafter, high IE temperatures (435–480 °C) decrease the elastic recovery at the edge. The sample exchanged at 420 °C has the most consistently large elastic recovery improvement, however the 390 °C sample has a slightly higher peak elastic recovery (excluding the 450 °C sample). This trend is closer to that seen in the compressive stress profile and face-on nano-indentation results; the sample exchanged at 390 °C should display the most enhanced mechanical response, while 405–420 °C should have a smaller, but broader improvement. It is surprising that the sample exchanged at 450 °C shows such an improvement in ω_e far into the case depth, however, it is only a consequence of the sample having an unexpectedly low Y in Fig. 4 probably due to

cracking.

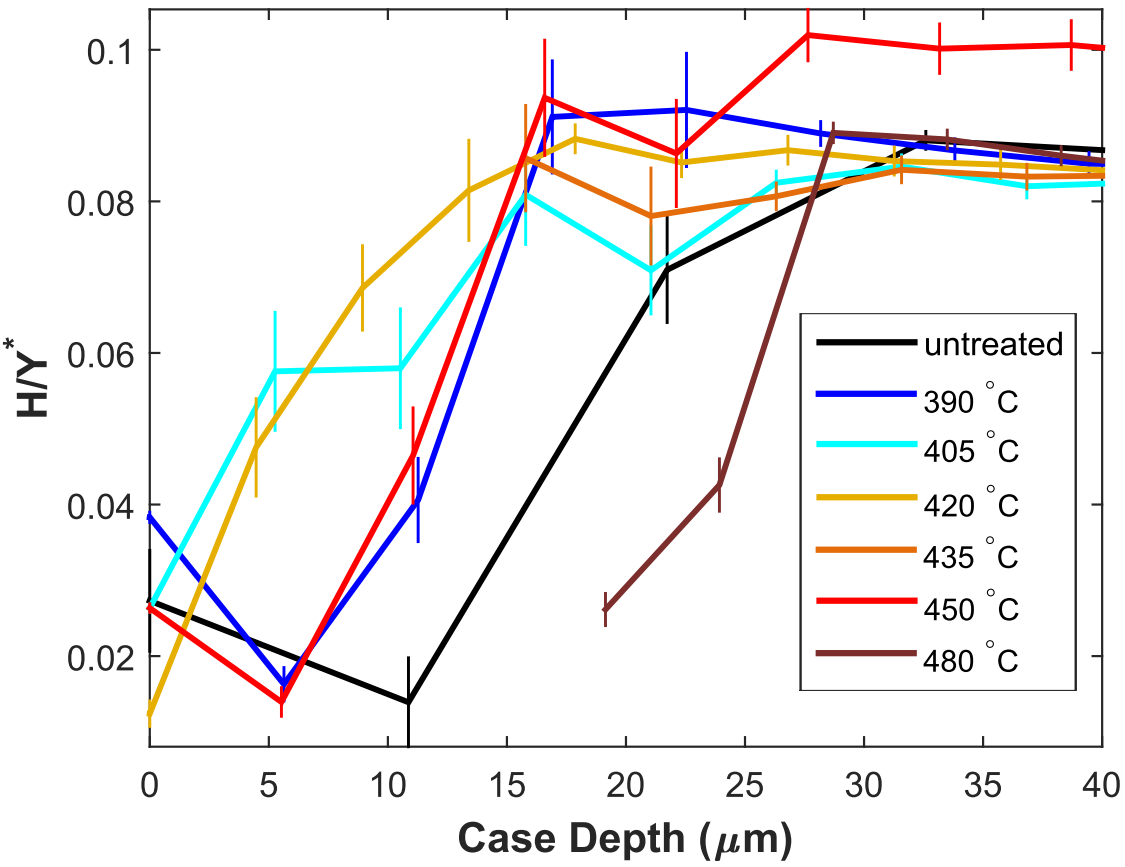

Figure 12: H/Y^*, which is proportional to elastic recovery (ω_e), as a function of case depth for all IE temperatures, 390–480 °C (dark blue–dark red) in comparison with the untreated lithium silicate glass (black). Only deep indent data (1500–2000 nm) were used.

The resistance to plastic deformation, H^3/Y^{*2}, shows similar trends (Fig. 13). Once more, with the exception of 480 °C, there is a positive relationship between enhanced mechanical response and increasing IE temperature. However, unlike elastic recovery which was roughly the same for all IE temperatures past a case depth of ≥ 30 μm, high IE temperature samples (435 and 480 °C) show decreased resistance to plastic deformation compared to the untreated sample in this region. Again, the sample exchanged at 450 °C shows an unexpected improvement in H^3/Y^{*2} far into the case depth. All the same, perhaps the effects of composition are observable here; when the sample relaxes more, the resistance to plastic deformation becomes more similar to that of the as-melted mixed-alkali composition

($20Li_2O$-$10K_2O$-$70SiO_2$). Finally, the sample exchanged at 420 °C has the highest resistance to plastic deformation at the immediate edge, however, the 390 °C sample has the highest H^3/Y^{*2} further into the case depth (excluding the 450 °C sample). Once again, this result corresponds more closely with the compressive stress profile.

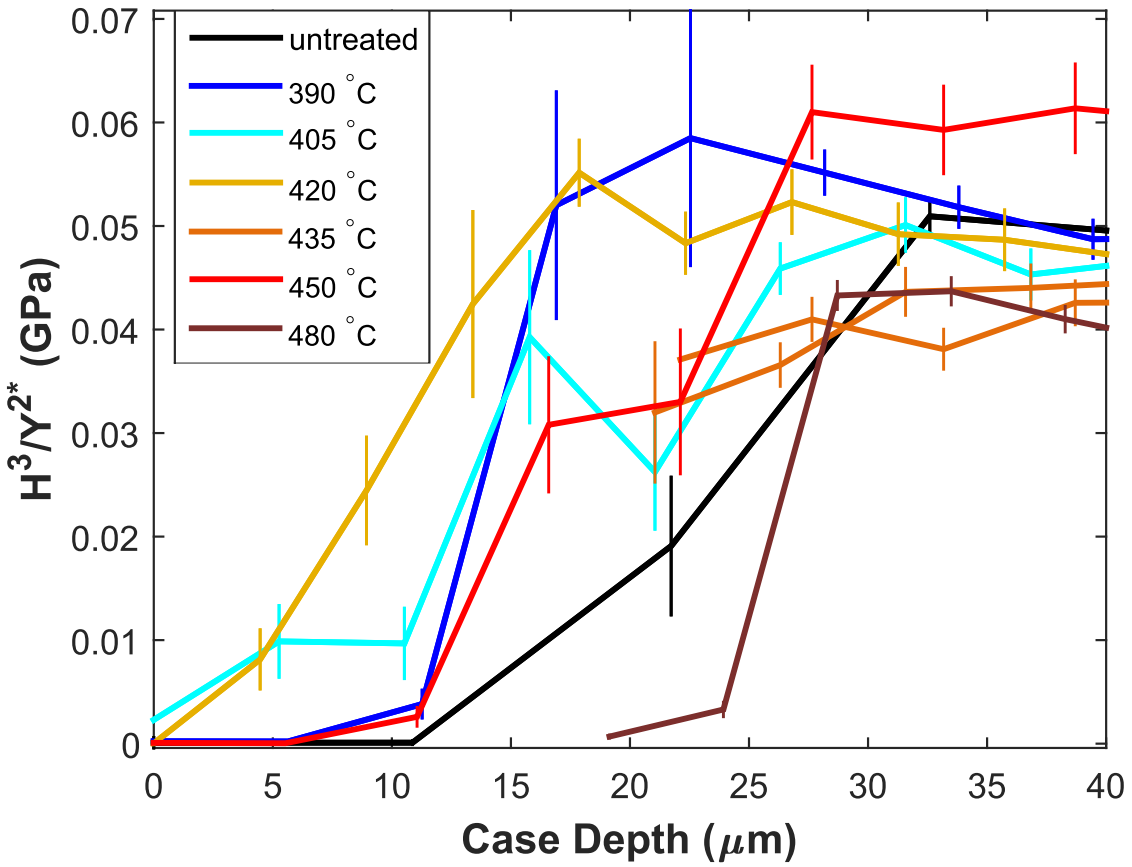

Figure 13: H^3/Y^{*2} (correlated with resistance to plastic deformation) as a function of case depth for all IE temperatures, 390–480 °C (dark blue–dark red) in comparison with the untreated lithium silicate glass (black). Only deep indent data (1500–2000 nm) were used.

Although it is difficult to observe in Figs. 12 and 13, the resistance to plastic deformation improves 2–3 times more than the elastic recovery near the edge for samples exchanged at low IE temperatures, 390–420 °C. This result agrees with our conclusion from the normalized Y/Y_0 and H/H_0 plots in Figs. 8 and 9. To better understand this result, it is important to realize H/Y^* is related to the maximum elastic strain, while H^3/Y^{*2} is related to the energy required for plastic deformation. Since brittle materials can only withstand small amounts

of strain until fracture, it may simply be that there is little opportunity to improve their elastic recovery. On the other hand, the amount of energy required for plastic deformation is more variable as it involves both stiffness and maximum strain. Nonetheless, it follows that in addition to arresting cracks due to compressive stress, IE also leads to the reduction in new flaws forming at the edge, which is expected from the high scratch resistance conferred by IE.

Additionally, unlike elastic recovery, H^3/Y^{*2} was found to be affected further away from the edge (> 30 μm) at high IE temperatures (435 and 480 °C). This is a result of high IE temperatures causing reduced hardness, likely because of having less compressive stress due to thermal relaxation. Overall, the improved scratch resistance, *i.e.* hardness, imparted from IE likely comes from the compressive stress at the edge mitigating tensile stresses, causing both crack closure and arresting in addition to decreasing shear flow. The MAE concurrently enhances hardness more than stiffness, thus, it may be improving mechanical properties by increasing elastic recovery and resistance to plastic deformation, in addition to increasing the fracture stress per Griffith's equation.[4]

The results from micro-indentation agree with those determined for elastic recovery and resistance to plastic deformation. Both H/Y and H^3/Y^{*2} displayed the most improvement nearest the edge (0–10 μm) in the samples exchanged at 405 and 420 °C, which are the same IE temperatures that saw enhanced micro-hardness. Additionally, IE temperature 390 °C did not show improvement in this region and the micro-hardness for this sample was found to be less than the untreated sample. Once more these results indicate the importance of the first 10–15 microns in determining the performance of the material.

Conclusion

Following ion exchange, significant improvements in stiffness and hardness were seen near the edge (0–30 μm) when exchange was performed at temperatures (390–435 °C) below T_g

(459 °C). Low IE temperatures (390 and 405 °C) resulted in better mechanical properties further into the case depth ($\geq$ 30 μm). Conversely, IE temperatures near or above T_g (450 and 480 °C) worsened mechanical properties near the edge as well as throughout the case depth. Low IE temperatures resulted in more compressive stress to oppose the concentrated tensile stress found at crack tips; this likely lead to a decrease in the importance of the surface condition and/or crack closure, causing an enhancement of mechanical properties near the edge. On the other hand, high IE temperatures caused relaxed structures similar to the as-melted, mixed-alkali series and little compressive stress; as a result, the surface condition is as important in these glasses as it is in the untreated composition, thus, the mechanical properties are not improved. Essentially, the IE process was observed to negate the free edge effect and restore the mechanical properties near the edge to those found in the middle of the specimen.

Overall, the hardness results from side-view nano-indentation were found to agree well with those from micro-indentation, namely the samples exchanged at 405 and 420 °C showed the most improved H near the edge. This agreement demonstrates the applicability of the stiffness results from nano-indentation measurements to the micron scale as well, which is an important, yet difficult property to measure in a thin layer. Considering that in the case of glass, the response at the edge is a large predictor of the material performance, understanding which properties are improved near the edge may help model the mechanical response due to the IE process.

Despite the 405 and 420 °C samples having the most enhanced mechanical properties, they are known to have lower compressive stresses (over a larger case depth) than the sample exchanged at 390 °C. Consequently, the improvements in Y and H cannot be fully explained in terms of compressive stress and thermal relaxation alone. Hardness was seen to be greatly enhanced by the IE process, however, stiffness was improved beyond that which was expected from compressive stress alone, revealing that the MAE plays a role in the improvement of both mechanical properties. Given the composition dependence of the mechanical properties,

it may be worth investigating the magnitude of the MAE in prospective IE materials.

The indent size was also found to effect stiffness and hardness, especially close to the edge due to the free edge effect. Interestingly, trends observed for shallow indents were more similar to those expected from compressive stress profiles, which may indicate release of compression with increasing indent depth. Moreover, this ISE-like behaviour was more pronounced for low IE temperatures in comparison to the untreated and high IE temperature samples, likely because low IE temperatures have more compression to be relaxed by indentation.

When the mechanical properties were evaluated in terms of elastic recovery (H/Y^*) and resistance to plastic deformation (H^3/Y^{*2}), the effect of IE temperature on these two responses matched the compression profiles: IE temperature 390 °C had the most enhanced mechanical response, while 420 °C had a less improved response over a larger case depth, especially near the edge. Overall, both responses were seen to improve by the IE process, however, the plastic response was found to be more enhanced compared to the elastic response. This likely contributes to the high scratch resistance observed in IE glasses where a decrease in plastic flow reduces the likelihood of new flaws from occurring. Stiffness appears to act in two different ways: first by increasing the magnitude of compressive stress, yet also by decreasing elastic recovery and resistance to plastic deformation during indentation. Although the IE process improves hardness more than stiffness, only stiffness plays a role in the magnitude of compressive stress found in the IE layer; thus, stiffness is important when considering surface mechanics.

Associated Content

Supporting Information

This material is available free of charge at http://pubs.acs.org/. Graphs of Young's modulus versus displacement into surface for multiple replicas; graphs of Young's modulus and

hardness versus displacement into surface for different locations from edge, for samples at increasingly higher ion exchange temperatures.

Acknowledgement

Financial support from the Natural Sciences and Engineering Research Council of Canada (Canada Grant Number RGPIN 261987) is gratefully acknowledged. The authors thank Prof. Daniel Boyd for use of the nano-indentation instrument and Prof. Kevin Plucknett for use of the micro-indenter. Finally, we would like to thank Dr. Carl Romao for helpful discussions.

References

(1) Wondraczek, L.; Mauro, J. C.; Eckert, J.; Kühn, U.; Horbach, J.; Deubener, J.; Rouxel, T. Towards Ultrastrong Glasses. *Adv. Mater.* **2011**, *23*, 4578–4586.

(2) Phillips, C. J. The Strength and Weakness of Brittle Materials. *Am. Sci.* **1965**, *53*, 20–51.

(3) Inglis, C. Stress in a Plate due to the Presence of Sharp Corners and Cracks. *Trans. Roy. Inst. Naval Architects* **1913**, *60*, 219–241.

(4) Griffith, A. A. The Phenomena of Rupture and Flow in Solids. *Philos. Trans. R. Soc., A* **1921**, *221*, 163–198.

(5) Gy, R. Ion Exchange for Glass Strengthening. *Mater. Sci. Eng. B* **2008**, *149*, 159–165.

(6) Suszynska, M. Load Dependence of Hardness of the Doped Soda-Lime Silicate Glasses. *Opt. Appl.* **2012**, *42*, 399–406.

(7) Svenson, M. N.; Thirion, L. M.; Youngman, R. E.; Mauro, J. C.; Rzoska, S. J.; Bockowski, M.; Smedskjær, M. M. Pressure-induced Changes in Interdiffusivity and Com-

pressive Stress in Chemically Strengthened Glass. *ACS Appl. Mater. Inter.* **2014**, *6*, 10436–44.

(8) Rogoziński, R. In *Ion Exchange Technologies*; Kilislioğlu, A., Ed.; Intech, 2012; pp 154–190.

(9) Stavrou, E.; Palles, D.; Kamitsos, E. I.; Lipovskii, A.; Tagantsev, D.; Svirko, Y.; Honkanen, S. Vibrational Study of Thermally Ion-exchanged Sodium Aluminoborosilicate Glasses. *J. Non-Cryst. Solids* **2014**, *401*, 232–236.

(10) Varshneya, A. K. Chemical Strengthening of Glass: Lessons Learned and Yet To Be Learned. *Int. J. Appl. Glass Sci.* **2010**, *1*, 131–142.

(11) Quaranta, A.; Rahman, A.; Mariotto, G.; Maurizio, C.; Trave, E.; Gonella, F.; Cattaruzza, E.; Gibaudo, E.; Broquin, J. E. Spectroscopic Investigation of Structural Rearrangements in Silver Ion-Exchanged Silicate Glasses. *J. Phys. Chem. C* **2012**, *116*, 3757–3764.

(12) Tandia, A.; Vargheese, K. D.; Mauro, J. C.; Varshneya, A. K. Atomistic Understanding of Network Dilation Anomaly in Ion-exchanged Glass. *J. Non-Cryst. Solids* **2012**, *358*, 316–320.

(13) Kreski, P. K.; Varshneya, A. K.; Cormack, A. N. Investigation of Ion-exchanged 'Stuffed' Glass Structures by MD. *J. Non-Cryst. Solids* **2012**, *358*, 3539–3545.

(14) Sane, A.; Cooper, A. Stress Buildup and Relaxation during Ion Exchange Strengthening of Glass. *J. Am. Ceram. Soc.* **1987**, *70*, 86–89.

(15) Varshneya, A. Kinetics of Ion Exchange in Glasses. *J. Am. Ceram. Soc.* **1975**, *19*, 355–365.

(16) Varshneya, A. K. Method for Making Strengthened Glass. 2015; US Patent 8,959,953.

(17) Popov, V. L. *Contact Mechanics and Friction, Physical Principle and Applications*; Springer-Verlag Berlin Heidelberg: Berlin, Germany, 2010; pp 3–42.

(18) Sakai, T.; Suzuki, M. Distribution Characteristics of Mechanical Properties and Correlation between the Respective Properties on S35C Carbon Steel. *J. Mater. Sci.* **1991**, *26*, 1755–1761.

(19) Oyen, M. L. Nanoindentation Hardness of Mineralized Tissues. *J. Biomech.* **2006**, *39*, 2699–2702.

(20) Moyhihan, C.; Saad, N.; Tran, D.; Lessikar, A. Mixed-alkali Effect in the Dilute Foreign–Alkali Region. Failure of the Strong Electrolyte. *J. Am. Ceram. Soc.* **1980**, *63*, 458–464.

(21) Mohajerani, A.; Zwanziger, J. Mixed Alkali Effect on Vickers Hardness and Cracking. *J. Non-Cryst. Solids* **2012**, *358*, 1474–1479.

(22) Ballaran, T. B. In *High-Pressure Crystallography: From Fundamental Phenomena to Technological Applications*; Boldyreva, E., Dera, P., Eds.; Springer Science: Berlin, 2010; pp 135–145.

(23) Hofmeister, A. M. Pressure Derivatives of the Bulk Modulus. *J. Geophys. Res.* **1991**, *96*, 21893.

(24) Li, X.; Bhushan, B. A Review of Nanoindentation Continuous Stiffness Measurement Technique and its Applications. *Mater. Charact.* **2002**, *48*, 11–36.

(25) Pharr, G. Measurement of Mechanical Properties by Ultra-low Load Indentation. *Mater. Sci. Eng. A* **1998**, *253*, 151–159.

(26) Pharr, G. M.; Herbert, E. G.; Gao, Y. The Indentation Size Effect: A Critical Examination of Experimental Observations and Mechanistic Interpretations. *Annu. Rev. Mater. Res.* **2010**, *40*, 271–292.

(27) Kaji, M.; Stevenson, M.; Bradt, R. Knoop Microhardness Anisotropy and the Indentation Size Effect on the Basal Plane of Single-Crystal Alumina (Sapphire). *J. Am. Ceram. Soc.* **2002**, *22*, 415–422.

(28) Jang, J.-I.; Yoo, B.-G.; Kim, Y.-J.; Oh, J.-H.; Choi, I.-C.; Bei, H. Indentation Size Effect in Bulk Metallic Glass. *Scripta Mater.* **2011**, *64*, 753–756.

(29) Li, N.; Liu, L.; Zhang, M. The Role of Friction to the Indentation Size Effect in Amorphous and Crystallized Pd-Based Alloy. *J. Mater. Sci.* **2009**, *44*, 3072–3076.

(30) Huang, Y.; Shen, J.; Sun, Y.; Sun, J. Indentation Size Effect of Hardness of Metallic Glasses. *Mater. Design* **2010**, *31*, 1563–1566.

(31) Manika, I.; Maniks, J. Size Effects in Micro- and Nanoscale Indentation. *Acta Mater.* **2006**, *54*, 2049–2056.

(32) Oliver, W. C.; Pharr, G. M. An Improved Technique for Determining Hardness and Elastic Modulus using Load and Displacement Sensing Indentation Experiments. *J. Mater. Res.* **1992**, *7*, 1564–1583.

(33) Li, H.; Bradt, R. C. The Indentation Load/Size Effect and the Measurement of the Hardness of Vitreous Silica. *J. Non-Cryst. Solids* **1992**, *146*, 197–212.

(34) Ebisu, T.; Horibe, S. Analysis of the Indentation Size Effect in Brittle Materials from Nanoindentation Load-Displacement Curve. *J. Eur. Ceram. Soc.* **2010**, *30*, 2419–2426.

(35) Greaves, G. N. Poisson's Ratio Over Two Centuries: Challenging Hypotheses. *Notes and Recs. Royal Soc.* **2012**, *21*, 1–22.

(36) Jakes, J. E.; Stone, D. S. The Edge Effect in Nanoindentation. *Philos. Mag.* **2011**, *91*, 1387–1399.

(37) Jebahi, M.; André, D.; Dau, F.; Charles, J. L.; Iordanoff, I. Simulation of Vickers Indentation of Silica Glass. *J. Non-Cryst. Solids* **2013**, *378*, 15–24.

(38) Yaghoubi, H.; Taghavinia, N.; Alamdari, E. K.; Volinsky, A. A. Nanomechanical Properties of TiO_2 Granular Thin Films. *ACS Appl. Mater. Inter.* **2010**, *2*, 2629–2636.

(39) Newey, D.; Wilkins, M.; Pollock, H. An Ultra-Low-Load Penetration Hardness Tester. *J. Phys. E: Sci. Instr.* **1982**, *15*, 119.

(40) Jakes, J.; Frihart, C.; Beecher, J.; Moon, R.; Stone, D. Experimental Method to Account for Structural Compliance in Nanoindentation Measurements. *J. Mater. Res.* **2008**, *23*, 1113–1127.

(41) Jakes, J.; Frihart, C.; Beecher, J.; Moon, R.; Resto, P.; Melgarejo, Z.; Suárez, O.; Baumgart, H.; Elmustafa, A.; Stone, D. Nanoindentation near the Edge. *J. Mater. Res.* **2009**, *24*, 1016–1031.

(42) Downing, T.; Kumar, R.; Cross, W.; Kjerengtroen, L.; Kellar, J. Determining the Interphase Thickness and Properties in Polymer Matrix Composites using Phase Imaging Atomic Force Microscopy and Nanoindentation. *J. Adhes. Sci. Technol.* **2000**, *14*, 1801.

(43) Hodzic, A.; Stachurski, Z. H.; Kim, J. K. Nano-indentation of Polymer–Glass Interfaces Part I. Experimental and Mechanical Analysis. *Polymer* **2000**, *41*, 6895–6905.

(44) Zong, Z.; Lou, J.; Adewoye, O. O.; Elmustafa, A. A.; Hammad, F.; Soboyejo, W. O. Indentation Size Effects in the Nano- and Micro-Hardness of fcc Single Crystal Metals. *Mater. Sci. Eng. A* **2006**, *434*, 178–187.

(45) Wellman, R. G.; Dyer, A.; Nicholls, J. R. Nano and Micro Indentation Studies in Bulk Zirconia and EB PVD TBCs. *Surf. Coat. Tech.* **2003**, *174–175*, 720–724.

(46) Green, D. J. Compressive Surface Strengthening of Brittle Materials by a Residual Stress Distribution. *J. Am. Ceram. Soc.* **1983**, *66*, 807–810.

(47) Striepe, S.; Smedskjær, M. M.; Deubener, J.; Bauer, U.; Behrens, H.; Potuzak, M.; Youngman, R. E.; Mauro, J. C.; Yue, Y. Elastic and Micromechanical Properties of

Isostatically Compressed Soda-Lime-Borate Glasses. *J. Non-Cryst. Solids* **2013**, *364*, 44–52.

(48) Wu, J.; Deubener, J.; Stebbins, J. F.; Grygarova, L.; Behrens, H.; Wondraczek, L.; Yue, Y. Structural Response of a Highly Viscous Aluminoborosilicate Melt to Isotropic and Anisotropic Compressions. *J. Chem. Phys.* **2009**, *131*, 104504.

(49) Smedskjær, M. M.; Mauro, D. J.; Sen, S.; Yue, Y. Quantitative Design of Glassy Materials Using Temperature-Dependent Constraint Theory. *Chem. Mater.* **2010**, *2*, 445–452.

(50) Bridgman, P. W.; Simon, I. Effects of Very High Pressures on Glass. *J. Appl. Phys.* **1953**, *24*, 405.

(51) Bull, S. On the Origins of the Indentation Size Effect. *Z. Metallkd.* **2003**, *94*, 787–792.

(52) Liu, Y.; Ngan, A. Depth Dependence of Hardness in Copper Single Crystals Measured by Nano-Indentation. *Scr. Mater.* **2001**, *44*, 237–241.

(53) Durst, K.; Backes, B.; Göken, M. Indentation Size Effect in Metallic Materials: Correcting for the Size of the Plastic Zone. *Scr. Mater.* **2005**, *52*, 1093–1097.

(54) Pathak, S.; Stojakovic, D.; Doherty, R.; Kalidindi, S. Importance of Surface Preparation on the Nano- Indentation Stress-Strain Curves Measured in Metals. *J. Mater. Res.* **2009**, *24*, 1142–1155.

(55) Musil, J.; Kunc, F.; Zeman, H.; Poláková, H. Relationships between Hardness, Young's Modulus and Elastic Recovery in Hard Nanocomposite Coatings. *Surf. Coat. Tech.* **2002**, *154*, 304–313.

(56) Chiang, S. S.; Marshall, D. B.; Evans, A. G. The Response of Solids to Elastic/Plastic Indentation. I. Stresses and Residual Stresses. *J. Appl. Phys.* **1982**, *53*, 298.

(57) Johnson, K. L. *Contact Mechanics*; Cambridge University Press: Cambridge, UK, 1985; p 452.

(58) Tsui, T. Y.; Pharr, G. M.; Oliver, W. C.; Bhatia, C. S.; White, R. L.; Anders, S.; Anders, A.; Brown, I. G. Mechanical Behaviour of Diamond and other Forms of Carbon. *Mat. Res. Soc. Symp. Proc.* **1995**, *383*, 447–452.

Graphical TOC Entry

Nano-indentation Study of the Surface of Ion-Exchanged Lithium Silicate Glass

Courtney Calahoo, Xiaofang Zhang and J. W. Zwanziger